

# Caustic Skeleton & Cosmic Web

**Job Feldbrugge<sup>a</sup> Rien van de Weygaert<sup>b</sup> Johan Hidding<sup>b,c</sup> Joost Feldbrugge<sup>d</sup>**

<sup>a</sup>Perimeter Institute for Theoretical Physics, University of Waterloo,  
Waterloo, Canada

<sup>b</sup>Kapteyn Astronomical Institute, University of Groningen,  
Groningen, The Netherlands

<sup>c</sup>Netherlands eScience Center, Amsterdam, The Netherlands

<sup>d</sup>JFA Feldbrugge Studios,  
Lettelbert, The Netherlands

E-mail: [jfeldbrugge@perimeterinstitute.ca](mailto:jfeldbrugge@perimeterinstitute.ca)

## Abstract.

We present a general formalism for identifying the caustic structure of a dynamically evolving mass distribution, in an arbitrary dimensional space. For the class of Hamiltonian fluids the identification corresponds to the classification of singularities in Lagrangian catastrophe theory. On the basis of this formalism we develop a theoretical framework for the dynamics of the formation of the cosmic web, and specifically those aspects that characterize its unique nature: its complex topological connectivity and multiscale spinal structure of sheetlike membranes, elongated filaments and compact cluster nodes.

The present work represents a significant extension of the work by Arnol'd et al. [10], who classified the caustics that develop in one- and two-dimensional systems that evolve according to the Zel'dovich approximation. His seminal work established the defining role of emerging singularities in the formation of nonlinear structures in the universe. At the transition from the linear to nonlinear structure evolution, the first complex features emerge at locations where different fluid elements cross to establish multistream regions. Involving a complex folding of the 6-D sheetlike phase-space distribution, it manifests itself in the appearance of infinite density caustic features. The classification and characterization of these mass element foldings can be encapsulated in *caustic conditions* on the eigenvalue and eigenvector fields of the deformation tensor field.

In this study we introduce an alternative and transparent proof for Lagrangian catastrophe theory. This facilitates the derivation of the caustic conditions for general Lagrangian fluids, with arbitrary dynamics, and even including dissipative terms and vorticity. Most important in the present context is that it allows us to follow and describe the full three-dimensional geometric and topological complexity of the purely gravitationally evolving nonlinear cosmic matter field. While generic and statistical results can be based on the eigenvalue characteristics, one of our key findings is that of the significance of the *eigenvector field* of the deformation field for outlining the entire spatial structure of the *caustic skeleton* emerging from a primordial density field.

In this paper we explicitly consider the caustic conditions for the three-dimensional Zel'dovich approximation, extending earlier work on those for one- and two-dimensional fluids towards the full spatial richness of the cosmic web. In an accompanying publication, we apply this towards a full three-dimensional study of caustics in the formation of the cosmic web and evaluate in how far it manages to outline and identify the intricate skeletal features in the corresponding  $N$ -body simulations.

---

## Contents

<b>1</b>	<b>Introduction</b>	<b>1</b>
<b>2</b>	<b>Lagrangian fluid dynamics</b>	<b>4</b>
2.1	Hamiltonian fluid dynamics	6
<b>3</b>	<b>Shell-crossing conditions</b>	<b>6</b>
3.1	Shell-crossing condition: the derivation	7
3.2	Shell-crossing condition: theorems	10
3.3	Shell-crossing conditions: significance	11
3.4	Shell-crossing conditions: coordinate transformation	11
<b>4</b>	<b>Caustic conditions</b>	<b>12</b>
4.1	The $A$ family	14
4.1.1	The trivial $A_1$ class	15
4.1.2	The $A_2$ caustics	15
4.1.3	The $A_3$ caustics	15
4.1.4	The $A_3^\pm$ points	16
4.1.5	The $A_4$ caustics	19
4.1.6	The $A_4^\pm$ points	21
4.1.7	The $A_5$ caustics	21
4.2	The $D$ family	22
4.2.1	The $D_4$ caustics	22
4.2.2	The $D_4^\pm$ points	26
4.2.3	The $D_5$ caustics	26
<b>5</b>	<b>Classification of singularities</b>	<b>27</b>
5.1	Classes of Lagrangian fluids	27
5.2	Singularity classification	28
5.3	Singularity classification: generic fluids	29
5.4	Singularity classification: Hamiltonian fluids	30
5.5	Unfoldings	32
5.6	Density profile	32
<b>6</b>	<b>The caustic skeleton &amp; the cosmic web</b>	<b>32</b>
6.1	Higher order Lagrangian perturbations	38
6.2	Gaussian statistics of the caustic skeleton	38
<b>7</b>	<b>Dynamics and evolution of caustics</b>	<b>39</b>
7.1	Caustic mutations and transformations: evolutionary sequence	40
7.2	Singularity transformations	41
7.2.1	Evolving $A$ -family caustics	41
7.2.2	Evolving $D$ -family caustics	42
<b>8</b>	<b>Discussion &amp; Conclusions</b>	<b>42</b>

<b>A</b>	<b>Zel'dovich approximation</b>	<b>50</b>
<b>B</b>	<b>Lagrangian maps and Lagrangian equivalence</b>	<b>51</b>
B.1	Symplectic manifolds and Lagrangian maps	51
B.2	Displacement as Lagrangian map	52
B.3	Lagrangian map germs	52
B.4	Gradient maps	53
B.5	Arnol'd's classification of Lagrangian catastrophes	54
<b>C</b>	<b>Caustic conditions of the normal forms</b>	<b>54</b>

---

## 1 Introduction

Caustics are important features in the dynamics of fluids, marking the positions where fluid elements cross and multi-stream regions form. The caustics can be associated to the regions with infinite density, corresponding to locations where shell-crossing occurs or where we see the formation of shocks. In the study presented, we concentrate specifically on the role of caustics in the formation of the cosmic web. Notwithstanding this focus, the caustic conditions and mathematical formalism that we have derived for this are of a far more generic nature, whose validity is independent of the dynamics of the fluid described.

The cosmic web is the complex network of interconnected filaments and walls into which galaxies and matter have aggregated on Megaparsec scales. It contains structures from a few megaparsecs up to tens and even hundreds of megaparsecs of size. Its appearance has been most dramatically illustrated by the maps of the nearby cosmos produced by large galaxy redshift surveys such as the 2dFGRS, the SDSS, and the 2MASS redshift surveys [26, 42, 66], as well as by recently produced maps of the galaxy distribution at larger cosmic depths such as VIPERS [37]. The weblike spatial arrangement is marked by highly elongated filamentary and flattened planar structures, connecting in dense compact cluster nodes surrounding large near-empty void regions.

The Cosmic Web is one of the most striking examples of complex geometric patterns found in nature, and certainly the largest in terms of size. According to the *gravitational instability scenario* [55], cosmic structure grows from tiny primordial density and velocity perturbations. Once the gravitational clustering process has progressed beyond the initial linear growth phase, we see the emergence of complex patterns and structures in the density field. As borne out by a large sequence of N-body computer experiments of cosmic structure formation (e.g. [60, 65, 70]), web-like patterns in the overall cosmic matter distribution do represent a universal but possibly transient phase in the gravitationally driven emergence and evolution of cosmic structure (see e.g. [4, 22]). N-body calculations have shown that web-like patterns defined by prominent anisotropic filamentary and planar features — and with characteristic large underdense void regions — are a natural manifestation of the gravitational cosmic structure formation process. The recognition of the *Cosmic Web* as a key aspect in the emergence of structure in the Universe came with early analytical studies and approximations concerning the emergence of structure out of a nearly featureless primordial Universe. In this respect the Zel'dovich formalism [73] played a seminal role.

The emphasis on anisotropic collapse as agent for forming and shaping structure in the Zel'dovich "pancake" picture [43, 73] was seen as the rival view to the purely hierarchical clustering view of structure formation. The successful synthesis of both elements in the

*Cosmic Web* theory of Bond et al. [14] appears to provide a successful description of large scale structure formation in  $\Lambda$ CDM cosmology. It stresses the dominance of filamentary shaped features and emphasizes the intimate dynamical relationship between the filamentary patterns and the compact dense clusters that stand out as the nodes within the cosmic matter distribution [14, 24, 67]. It also indicates that a full understanding of its dynamical evolution should clarify how the various emerging structural features connect up in the intricate network of the cosmic web. To answer this question we need to turn to a full phase-space description of the evolving matter distribution and mass flows.

The Zel'dovich formalism [73] already underlined the importance of a full phase-space description for understanding cosmic structure formation, however, with the exception of a few prominent studies [10], the wealth of information content of full 6-D phase-space escaped attention. This changed with the publication of a number of recent publications [1, 30, 54, 58, 62] (for an early study on this observation see [20]). They realized that the morphology of components in the evolving matter distribution is closely related to its multistream character. This realization is based on the recognition that the emergence of nonlinear structures occurs at locations where different streams of the corresponding flow field cross each other.

Looking at the appearance of the evolving spatial mass distribution as a 3D *phase space sheet* folding itself in 6D phase space, a connection is established between the structure formation process and the morphological classification of the emerging structure. Based on these recent advances and insights, in this study we discuss the role of caustics in the formation of the cosmic web. The caustics mark the regions where non-linear gravitational collapse starts to take place and the cosmic web begins to form. By tracing the caustics during the formation of the cosmic web we obtain a skeleton of the current three-dimensional large scale structure.

Caustics in Lagrangian fluids with Hamiltonian dynamics are classified by Lagrangian catastrophe theory [6, 8, 47, 72]. These results were soon extended to fluids with generic dynamics [16]. For the classification of caustics emerging in the context of a one- and two-dimensional description of cosmic structure formation by the Zel'dovich approximation, Arnol'd et al. [10] translated this into conditions on the displacement field. Following up on this seminal work, Hidding et al. [39] analyzed the overall morphology and connectivity of caustics that emerge in a displacement field described by the one- and two-dimensional Zel'dovich approximation. The visual illustration of the emerging structure, for a field of initially Gaussian random density and potential fluctuations, revealed how the caustics spatially outline the spine of the cosmic web. Feldbrugge et al. [31] elaborated this into an analytical evaluation of the statistical properties of caustics, assuming a random Gaussian initial density field.

In the current study, we give a novel proof of Lagrangian catastrophe theory and the corresponding *caustic conditions* for three-dimensional Hamiltonian fluids. These conditions are expressed in both the eigenvalue and the eigenvector fields of the deformation tensor. Moreover, our scheme allows us to extend these caustic conditions to fluids with arbitrary dynamics in a space of arbitrary dimension. This in particular allows us to consider dissipative fluids for which the displacement field is not necessarily the gradient of a potential field. Applied to the three-dimensional Zel'dovich approximation, these conditions on the initial density field lead to a *caustic skeleton* of the cosmic web. In this skeleton the walls, filaments and clusters of the large scale structure are directly related to the  $A_3, A_4, A_5, D_4$  and  $D_5$  caustics of Lagrangian catastrophe theory. See figure 1 for an illustration of the caustic skeleton of the Zel'dovich approximation and a dark matter  $N$ -body simulation. A detailed

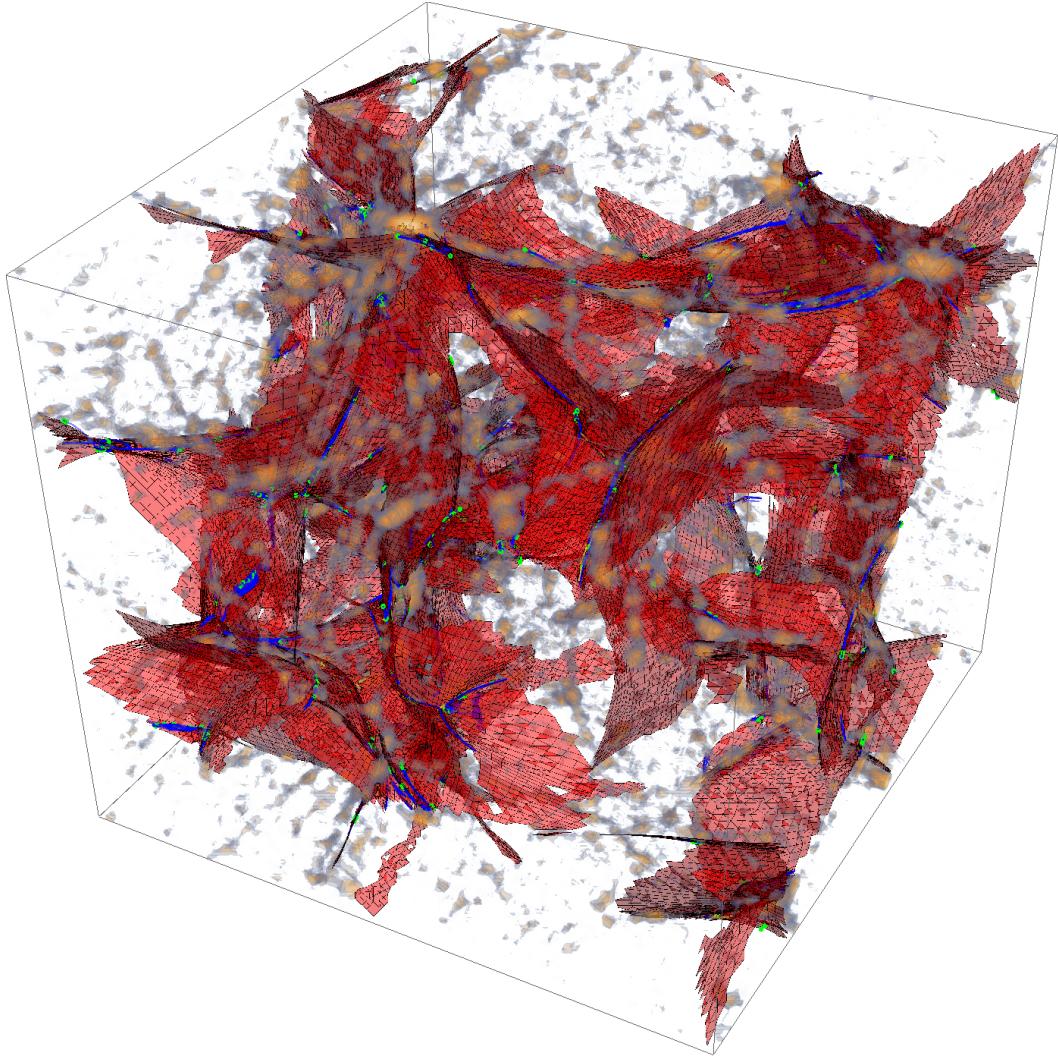


**Figure 1:** The log density field of a dark matter  $N$ -body simulation in a Einstein universe and cusp ( $A_3$ ), swallowtail ( $A_4$ ) and butterfly ( $A_5$ ) elements of the caustic skeleton corresponding to the lowest eigenvalue field. The red sheets represent the cusps ( $A_3$ ) singularities which correspond to the walls or membranes of the cosmic web. The blue lines and the green points are the swallowtail ( $A_4$ ) and butterfly ( $A_5$ ) singularities corresponding to the filaments and clusters of the large scale structure.

analysis of the caustic skeleton of the Zel'dovich approximation and a comparison with a  $N$ -body simulation is the subject of an accompanying paper [32].

It should be emphasized that the eigenvalue fields of the deformation tensor have, for a long time, been successfully used in Lagrangian studies of the cosmic web [23, 50, 71]. In these studies, the clusters, filaments and walls are related to the number of eigenvalues exceeding a threshold. The here proposed caustic skeleton complements their work in that it include the information of the eigenvector fields, which so far has been largely neglected.

The plan for the present paper starts with section 2, in which we give a concise description of Lagrangian fluid dynamics. The formation of caustics and derivation of the shell-crossing conditions is studied in section 3. These conditions are among the main results presented

here. In section 4 we apply these shell-crossing conditions to the classification of catastrophes, described in section 5, to derive the caustic conditions. Finally, in section 7 we describe the dynamical framework resulting from the considerations above.

## 2 Lagrangian fluid dynamics

There exist multiple approaches to fluid dynamics. In the Eulerian approach, the evolution of the smoothed density and velocity fields is analyzed. The equations of motion of Eulerian fluids are relatively concise and give a reasonably accurate description of the mean flow in a fluid element at a given location in the fluid.

One serious disadvantage of the Eulerian framework is that it does not directly relate to the motion of the particles in the fluid. Because it basically restricts itself to the mean motion in a fluid element, it does not facilitate an accurate description of the evolution of multi-stream regions. More suited for following the complex dynamical evolution of fluid elements, including the emergence of caustics, is the Lagrangian approach to fluid dynamics.

In Lagrangian fluid dynamics, we assume every point in space to consist of a mass element. These mass elements flow with the fluid. Their motion is described by a map  $x_t : L \rightarrow E$ , mapping the initial position  $q$  in the Lagrangian manifold  $L$  to the position  $x_t(q)$  of the mass element in the Eulerian manifold  $E$  at time  $t$ . In the context of Lagrangian fluid dynamics, it is most convenient to describe the evolving fluid in terms of the displacement map  $s_t$  defined by,

$$s_t(q) = x_t(q) - q, \quad (2.1)$$

for all  $q \in L$ . For the Zel'dovich approximation [73] of cosmic structure formation the displacement field is given by

$$s_t(q) = -b_+(t)\nabla_q \Psi(q), \quad (2.2)$$

with the growing mode  $b_+$  and the displacement potential  $\Psi$ . The displacement potential is proportional to the linearly extrapolated gravitational potential to the current epoch  $\phi_0$ , *i.e.*

$$\Psi(q) = \frac{2}{3\Omega_0 H_0^2} \phi_0(q), \quad (2.3)$$

with  $H_0$  the current Hubble parameter and  $\Omega_0$  the current total energy density. In this paper we always assume the maps  $x_t$  and  $s_t$  to be continuous and sufficiently differentiable. While in the Lagrangian description a mass element has a constant mass, it may contract, expand, deform and even rotate. This is described in terms of the deformation tensor  $\mathcal{M}$ , the gradient of the displacement field with respect to the Lagrangian coordinates of a mass element,

$$\mathcal{M} = \frac{\partial s_t}{\partial q} = \begin{pmatrix} M_{1,1} & M_{2,1} & M_{3,1} \\ M_{1,2} & M_{2,2} & M_{3,2} \\ M_{1,3} & M_{2,3} & M_{3,3} \end{pmatrix}. \quad (2.4)$$

While mass elements in a Lagrangian fluid are characterized by a few fundamental quantities, which characterize them and remain constant throughout their evolution, most physical properties are basically derived quantities. A good example and illustration of a derived quantity is the density field. The density in a point  $x' \in E$  is defined as the initial mass in the mass

element times the ratio of the initial and final volume of the mass element. Formally, this is expressed as a change of coordinates involving the Jacobian of the map  $x_t$ ,

$$\begin{aligned}\rho(x', t) &= \sum_{q \in A_t(x')} \rho_i(q) \left| \frac{\partial x_t(q)}{\partial q} \right|^{-1} \\ &= \sum_{q \in A_t(x')} \rho_i(q) \left| I + \frac{\partial s_t(q)}{\partial q} \right|^{-1} \\ &= \sum_{q \in A_t(x')} \frac{\rho_i(q)}{|1 + \mu_{t1}(q)| |1 + \mu_{t2}(q)| |1 + \mu_{t3}(q)|},\end{aligned}\tag{2.5}$$

with  $A_t(x')$  the points  $q$  in Lagrangian space  $L$  which map to  $x'$ , i.e.,  $A_t(x') = \{q \in L | x_t(q) = x'\}$ ,  $\rho_i$  the initial density field and  $\mu_{ti}$  the eigenvalue fields of the deformation tensor  $\mathcal{M}(q)$ <sup>1</sup>. The last equality in equation (2.6) applies to general deformation tensors, since the characteristic polynomial of the deformation tensor can be expressed in terms of the eigenvalues

$$\chi(\lambda) = \det \left[ \frac{\partial s_t}{\partial q} - \lambda I \right] = (\mu_{t1} - \lambda)(\mu_{t2} - \lambda)(\mu_{t3} - \lambda),\tag{2.6}$$

by which

$$\det \left[ I + \frac{\partial s_t}{\partial q} \right] = \chi(-1) = (1 + \mu_{t1})(1 + \mu_{t2})(1 + \mu_{t3}).\tag{2.7}$$

By substituting derived quantities like density in the, often more familiar, Eulerian fluid equations, we may obtain a closed set of differential equations for the Eulerian position  $x_t$  or the displacement map  $s_t$ .

Equation (2.5) applies to a fluid with three spatial dimensions. The arguments presented in this paper straightforwardly generalize to a Lagrangian fluid with an arbitrary number of spatial dimension. For simplicity, we will restrict explicit expressions to the 3-dimensional case<sup>2</sup>. It is straightforward to generalize equation (2.5) to  $d$ -dimensional fluids in  $d$ -dimensional space.

Of key importance is the implication of equation (2.5) that an infinite density occurs when a mass element is turned inside out. More formally stated, as we will see in section 3, an infinite density occurs when for at least one of the  $i = 1, \dots, d$ ,

$$1 + \mu_i = 0.\tag{2.8}$$

The regions, in which the mapping  $x_t$  becomes degenerate and the density becomes infinite are known as *folding*, *caustics* or *shocks*. They mark important features in the Lagrangian fluid and are the object of study in this paper. Note that for practical reasons in this paper we will sometimes suppress the time index of the eigenvalue fields, i.e.  $\mu_i = \mu_{ti}$ .

---

<sup>1</sup>Note that here we use the general convention to represent the deformation eigenvalue field, with  $\mu_i(q)$  the  $i$ -th eigenvalue of the deformation tensor,  $\mathcal{M}(q)$ . This differs from the usual convention in cosmology to use the time-independent representation of the deformation field in the context of the Zel'dovich approximation. Within this formalism, the eigenvalues  $\lambda_i(q)$  of the deformation field  $\psi_{ij} = \partial^2 \Psi(q)/\partial q_i \partial q_j$ , are related to the eigenvalues  $\mu_i(q)$  via the linear relation  $\mu_i(q, t) = -b_+(t)\lambda_i(q)$ , in which  $b_+(t)$  is the growing mode growth factor. See Appendix A for further details.

<sup>2</sup>Formally, it would be appropriate to describe the fluids as  $(d + 1)$ -dimensional fluids, a combination of their embedding in a  $d$ -dimensional space along with their evolution along time dimension  $t$ .

Throughout our study, we assume that the displacement map  $s_t$  is continuous and sufficiently differentiable. The corresponding eigenvalues are the roots of the characteristic polynomial of the matrix  $\mathcal{M} = \partial s_t / \partial q$ . Since the characteristic equation is a non-linear equation, in principle the eigenvalues could develop singularities and become non-differentiable. However, it can be shown that the eigenvalues can be ordered such that they are continuous. Furthermore the eigenvalues will be differentiable whenever the eigenvalues are distinct. When two eigenvalues coincide, the eigenvalue fields may become non-differentiable.

## 2.1 Hamiltonian fluid dynamics

For fluids moving with no dissipation of energy, the Hamiltonian formalism may be applied. Hamiltonian fluids have a potential velocity field

$$v = \nabla \phi \quad (2.9)$$

with the velocity potential  $\phi$ . The mass density  $\rho$  and the velocity potential serve as conjugate variables for the Hamiltonian  $\mathcal{H}$ , with the equations of motion

$$\begin{aligned} \frac{\partial \rho}{\partial t} &= +\frac{\delta \mathcal{H}}{\delta \phi} = -\nabla \cdot (\rho v), \\ \frac{\partial \phi}{\partial t} &= -\frac{\delta \mathcal{H}}{\delta \rho}. \end{aligned} \quad (2.10)$$

A simple example of a Hamiltonian is

$$\mathcal{H} = \int dx \left( \frac{1}{2} \rho (\nabla \phi)^2 + e(\rho) \right), \quad (2.11)$$

where  $e(\rho)$  is the internal energy as a function of density  $\rho$ . The first equation of motion in equation (2.10) is equivalent to the continuity equation, while the second equation implies the Euler equation

$$\frac{\partial v}{\partial t} + v \cdot \nabla v = -\frac{1}{\rho} \nabla p, \quad (2.12)$$

in which  $p$  is the pressure of the fluid. For a thorough discussion of fluid mechanics we refer to the seminal volumes of [34], [49], and [48]. For detailed and extensive treatments and analyses of Hamiltonian mechanics and Hamiltonian fluids, we refer to the reviews and textbooks by [7], [59], [53], and [9].

## 3 Shell-crossing conditions

The caustics mentioned above result from the folding of the fluid in phase space. At the initial time,  $t = 0$ , the fluid has not yet evolved. The displacement map  $s$  is therefore the zero map, i.e.,

$$s_0(q) = 0 \quad (3.1)$$

for all  $q \in L$ . The map  $x_0(q)$  is one-to-one, i.e. each Eulerian coordinate  $x$  corresponds to one Lagrangian position  $q$ . Throughout the entire volume, the fluid only contains single-stream regions. As the fluid evolves and nonlinearities start to emerge, we see the development of *multi-stream regions* in the fluid. At the boundary of a multi-stream region, the volume of a mass element vanishes and its density – following eqn. (2.5) – becomes infinite. At

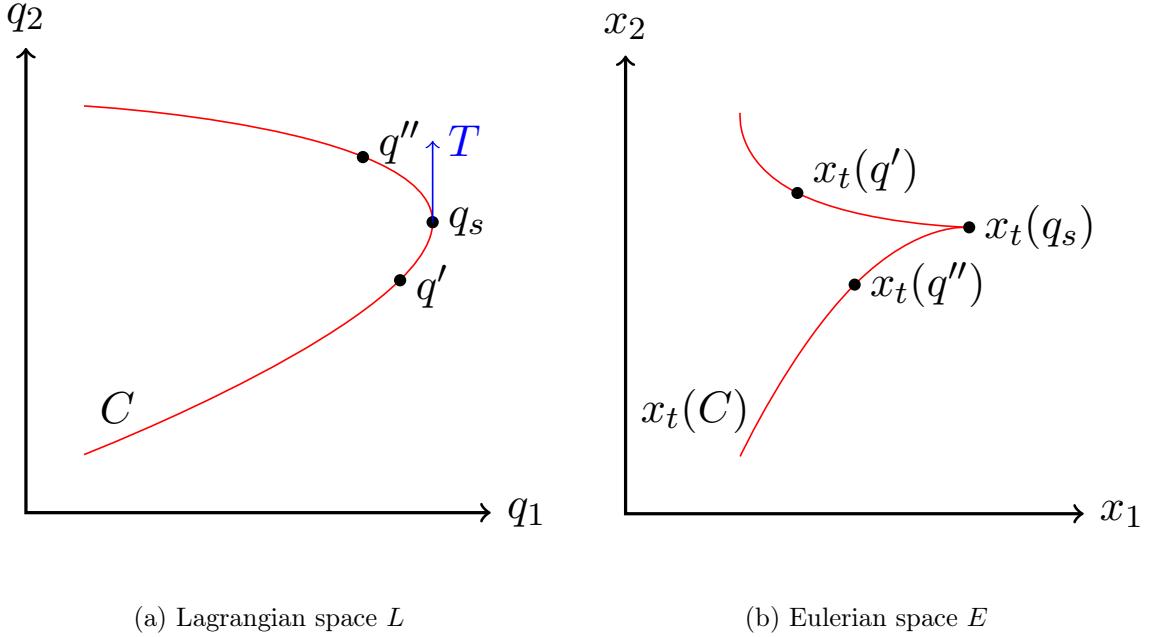


**Figure 2:** The shell-crossing process of a curve  $C$  in a Lagrangian map  $x_t$ . The left panel shows Lagrangian space, describing the initial positions of the fluid. The right panel shows Eulerian space, describing the positions of the fluid at time  $t$ . The fluid undergoes shell-crossing in point  $q_s$  on the curve  $C$  (red) at time  $t$ . The neighboring points  $q'$  and  $q''$  have passed through the opposing segments of  $C$ . The Lagrangian mapping of the curve  $x_t(C)$  (red) develops a non-differentiable point in  $x_t(q_s)$ , which is known as a caustic. The arrow  $T$  (blue) is the tangent vector of the curve  $C$  in point  $q_s$ .

such locations the map  $x_t(q)$  attains a  $n$ -to-one character, with  $n$  an odd positive integer ( $n = 3, 5, 7, \dots$ ). It means that at any one Eulerian location  $x$ , streams from  $n$  different Lagrangian positions cross.

The key question we address here is that of inferring the conditions under which a mass element with Lagrangian coordinate  $q$  undergoes shell-crossing. Here we derive the necessary and sufficient conditions for the process of shell-crossing to occur. These conditions are called *shell-crossing conditions*. They are the foundation on the basis of which we infer – in section 4 – the related conditions on the displacement field for the occurrence of the various classes of caustics. These are called the *caustic conditions*. We infer the caustic conditions for generic as well as Hamiltonian fluid dynamics.

### 3.1 Shell-crossing condition: the derivation

A typical configuration resulting from the *shell-crossing process* – the name by which it is usually indicated – is illustrated in figure 2. It focuses on points  $q = (q_1, q_2)$  that lie on a smooth curve  $C$  in Lagrangian space  $L$  (fig. 2a). At time  $t$ , the points on the Lagrangian curve  $C$  map to the variety  $x_t(C)$  in Eulerian space  $E$  (fig. 2b). The fluid in point  $q_s$  undergoes shell-crossing at time  $t$ . The neighboring points  $q'$  and  $q''$  have passed through the opposing segments of  $C$ . As a result of this, the curve  $C$  develops a non-differentiable point in  $x_t(q_s)$ , which is known as a *caustic*.

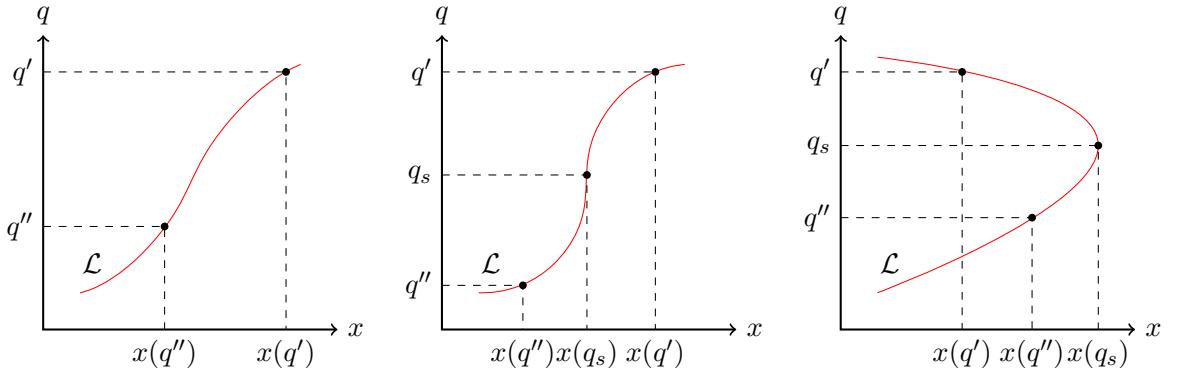


**Figure 3:** Folding of a one-dimensional fluid in phase space  $\mathcal{C}$ . The three panels show the time evolution of the Lagrangian submanifold  $\mathcal{L}$  (red) of the fluid in phase space. We track the evolution of two points  $(q', x(q'))$ ,  $(q'', x(q''))$  forming a multi-stream region and mark the point undergoing shell-crossing by  $(q_s, x(q_s))$ . Left panel: the fluid – early in its evolution – consisting of a single-stream region. Middle panel: a fluid during the process of shell-crossing. Right panel: a fluid consisting of a multi-stream region.

In a time sequence of three steps, figure 3 illustrates the dynamical process that is underlying the formation of the caustic at  $x_t(q_s)$ . The singularity at  $x_t(q_s) \in x_t(C)$  forms as the result of a folding process in phase space. We may appreciate the emerging structure when assessing the fate of two neighboring points  $q', q'' \in C$  on both sides of  $q_s$ . While the phase space sheet  $x_t(C)$  is folded, the points  $x_t(q')$  and  $x_t(q'')$  turn around while passing through  $x_t(q_s)$ . In figure 3 we observe how the initially single-stream phase space sheet (lefthand panel) morphs into a configuration marked by shell-crossing as different mass elements  $q$  pile up at the same Eulerian position  $x_t(q_s)$  (central panel). Subsequently, around  $x_t(q_s)$  we notice the formation of a multi-stream region, with the presence of mass elements  $q'$  having passed into a region where mass elements from other Lagrangian locations  $q$  are to be found.

To infer the shell-crossing conditions, we investigate a curve  $C$  in Lagrangian space along which we have points  $q$  that will find themselves incorporated in a singularity at Eulerian position  $x_s(q_s)$ . In the case of shell-crossing, points  $q$  near the Lagrangian location  $q_s$  will map onto the same Eulerian position  $x(q_s)$ . The key realization is that this occurs as points  $q$  along a direction  $T$  tangential to  $C$  are all folded on to a single Eulerian position  $x_s(q_s)$ . This translates the question of the shell-crossing condition into one on the identity of a tangential direction  $T(q)$  along which shell-crossing may or will occur. In other words, whether on a particular curve  $C$  – or, more general, a manifold  $M$  – there are points  $q$  where along one or more tangential directions  $T(q)$  to that curve or manifold shell-crossing may or will take place.

Zooming in on two points  $q'$  and  $q''$  in the vicinity of the singularity point  $q_s$ , we see that as a result of the folding process the ratio of the distances of the two points in the Lagrangian and Eulerian manifold, must go to zero in the limit that we zoom in on points  $q'$  and  $q''$  along the Lagrangian curve  $C$  at an infinitesimal distance from  $q_s$ , i.e.

$$\frac{\Delta x}{|\Delta q|} = \frac{\|x_t(q') - x_t(q'')\|}{\|q' - q''\|} \rightarrow 0 \quad q', q'' \rightarrow q_s . \quad (3.2)$$

The direct implication of this is, following equation (2.5), that the density in a caustic is

infinite: the volume of the mass element associated to  $q_s$  vanishes at time  $t$ . In essence it informs us that during shell crossing the points  $q$  near Lagrangian location  $q_s$ , along the tangential direction  $T$  to the Lagrangian curve  $C$ , map onto the same Eulerian position  $x(q_s)$ . This means that the norm of the directional derivative of  $x_t$  along the tangential direction vanishes. In other words, along the non-zero tangent vector  $T$  along  $C$ ,

$$\left\| \frac{\partial x_t}{\partial q} T \right\| = 0, \quad (3.3)$$

where  $\partial x_t / \partial q$  is the Jacobian of  $x_t$  evaluated in  $q_s$  (see figure 2a). This is equivalent to requiring that

$$\frac{\partial x_t}{\partial q} T = 0. \quad (3.4)$$

In terms of the displacement map  $s_t$ , this condition can be expressed as

$$T + \frac{\partial s_t}{\partial q} T = 0, \quad (3.5)$$

with the Jacobian  $\frac{\partial s_t}{\partial q}$  also evaluated in  $q_s$ <sup>3</sup>. Subsequently consider the eigenvalues  $\mu_i$  and eigenvectors  $v_i$  of the deformation tensor  $\mathcal{M} = \frac{\partial s_t}{\partial q}$ , defined by

$$\mathcal{M}v_i = \mu_i v_i. \quad (3.6)$$

We can construct the diagonal matrix  $\mathcal{M}_d = \text{diag}(\mu_1, \dots, \mu_d)$  and the eigenvector matrix  $\mathcal{V} = (v_1, \dots, v_d)$ . In three dimensions, with the eigenvalues  $\mu_i$  and eigenvectors  $v_i = (v_{i,1}, v_{i,2}, v_{i,3})$ , the diagonal matrix  $\mathcal{M}_d$  and eigenvector matrix  $\mathcal{V}$  are given by

$$\mathcal{M}_d = \begin{pmatrix} \mu_1 & 0 & 0 \\ 0 & \mu_2 & 0 \\ 0 & 0 & \mu_3 \end{pmatrix}, \quad \mathcal{V} = \begin{pmatrix} v_{1,1} & v_{2,1} & v_{3,1} \\ v_{1,2} & v_{2,2} & v_{3,2} \\ v_{1,3} & v_{2,3} & v_{3,3} \end{pmatrix}. \quad (3.7)$$

In terms of  $\mathcal{V}$  and  $\mathcal{M}_d$ , condition (3.5) reduces to

$$0 = (I + \mathcal{M})\mathcal{V}\mathcal{V}^{-1}T = \mathcal{V}(I + \mathcal{M}_d)\mathcal{V}^{-1}T \quad (3.8)$$

since  $\mathcal{V}$  is always invertible<sup>4</sup>, using the identity

$$\mathcal{M}\mathcal{V} = \mathcal{M}(v_1, \dots, v_d) = (\mathcal{M}v_1, \dots, \mathcal{M}v_d) = (\mu_1 v_1, \dots, \mu_d v_d) = \mathcal{V}\mathcal{M}_d. \quad (3.9)$$

We thus obtain the condition

$$(I + \mathcal{M}_d)\mathcal{V}^{-1}T = 0, \quad (3.10)$$

which holds for general deformation tensors and does not rely on whether the flow is potential (the deformation tensor is not assumed to be diagonalizable). Note that the rows of  $\mathcal{V}^{-1}$  consist of the dual vectors  $\{v_i^*\}$  of the eigenvectors  $\{v_i\}$ , defined by  $v_i \cdot v_j^* = \delta_{ij}$  for all  $i$  and  $j$ . Explicitly, this means that  $\mathcal{V}^{-1}$  in three dimensions is given by

$$\mathcal{V}^{-1} = \begin{pmatrix} v_{1,1}^* & v_{1,2}^* & v_{1,3}^* \\ v_{2,1}^* & v_{2,2}^* & v_{2,3}^* \\ v_{3,1}^* & v_{3,2}^* & v_{3,3}^* \end{pmatrix}, \quad (3.11)$$

---

<sup>3</sup>Unless mentioned otherwise, we will assume all Jacobians to be evaluated in  $q_s$ .

<sup>4</sup>That is to say, the eigenvectors can always be chosen to be linearly independent.

with  $v_i^* = (v_{i,1}^*, v_{i,2}^*, v_{i,3}^*)$ . The product  $\mathcal{V}^{-1}T$  is the vector composed out of the inner product of these dual vectors with the tangent vector  $T$ , so that in three dimensions equation (3.10) reduces to

$$\begin{pmatrix} (1 + \mu_1)v_1^* \cdot T \\ (1 + \mu_2)v_2^* \cdot T \\ (1 + \mu_3)v_3^* \cdot T \end{pmatrix} = 0. \quad (3.12)$$

This represents the proof for the shell-crossing condition for one-dimensional submanifolds. It states the condition for the tangential direction  $T$  along which Lagrangian points get folded into an Eulerian singularity point. The obtained condition is a telling expression for the central role of both the deformation eigenvalues and eigenvectors in determining the occurrence of a singularity.

### 3.2 Shell-crossing condition: theorems

Following the proof outlined in the previous subsection 3.1, we arrive at the following two theorems stipulating the conditions for the formation of singularities by curves  $C$  and arbitrary manifolds  $M$  in Lagrangian space  $L$ ,

**Theorem: 1** *A smooth curve  $C \subset L$  forms a singularity under the mapping  $x_t$  in the point  $x_t(q_s) \in x_t(C) \subset E$  if and only if*

$$(1 + \mu_{it}(q_s))v_{it}^*(q_s) \cdot T = 0 \quad (3.13)$$

*for all  $i$ , with  $T$  a nonzero tangent vector of  $C$  in  $q_s$ .*

For fluids with Hamiltonian dynamics (see sect 2.1) the Jacobian  $\partial s_t / \partial q$  is symmetric. The eigenvalues are real-valued and the eigenvectors can be taken to be orthonormal. The dual vectors of such a set of eigenvectors coincide with the eigenvectors, i.e.  $v_i^* = v_i$ .

It is important to note that the derived caustic conditions are general, and their validity independent of the dynamics of the fluid. At no point in our argument, we have made the assumption that the displacement field has to be a potential field. That is, more concretely, we have not based our derivation on the assumption that the deformation tensor is diagonalizable. For the intention to be able to apply the caustic formalism to general fluid dynamics this is critically important: fluids with non-Hamiltonian dynamics may have a Jacobian  $\partial s_t / \partial q$  with a non-vanishing anti-symmetric part. This implies fields of complex-valued eigenvalues, and a set of linearly independent (but not necessarily orthonormal) eigenvectors. Physically, it means that the fluid flow may also include vorticity components.

A similar argument holds for higher dimensional submanifolds of  $L$ , e.g., sheets and volumes. These manifolds can be  $n$ -dimensional, with  $n = 1, \dots, 3$  for three-dimensional fluids. Given an arbitrary manifold  $M \subset L$  we can consider all curves  $C \subset M$  passing through the point  $q_s \in M$ . The variety  $x_t(M)$  contains a singularity at  $x_t(q_s)$  if and only if at least one such curve  $C \subset M$  gets folded under the map  $x_t$ . Hence for an arbitrary submanifold

$M$ , we should consider the one-dimensional shell-crossing condition for all tangent vectors  $T$  in the vector space  $T_{q_s}M$  of all tangential vectors to the manifold  $M$  in  $q_s \in M$ <sup>5</sup>. This proves the general shell-crossing condition:

**Theorem: 2** *A manifold  $M \subset L$  forms a singularity under the mapping  $x_t$  in the point  $x_t(q_s) \in x_t(M) \subset E$  at time  $t$  if and only if there exists at least one nonzero tangent vector  $T \in T_{q_s}M$  satisfying*

$$(1 + \mu_{it}(q_s))v_{it}^*(q_s) \cdot T = 0 \quad (3.14)$$

for all  $i$ .

### 3.3 Shell-crossing conditions: significance

The shell-crossing conditions, as expressed in the two theorems above, are in agreement with our observation in section 2. That is, the conditions express the fact that caustics satisfy the sufficient and necessary condition  $1 + \mu_i = 0$  for at least one  $i$ .

This conclusion follows from the observation that if indeed at least for one  $i$  we have that  $1 + \mu_i = 0$ , we can always choose the vector  $T$  orthogonal to the span of eigenvectors  $\{v_j | j \neq i\}$ . For example, for the three-dimensional situation: if  $1 + \mu_1 = 0$ , we may chose the vector  $T$  to be orthogonal to the plane defined by the eigenvectors  $v_2$  and  $v_3$ . Along the direction of  $T$  we see the Lagrangian points  $q$  end up in a singularity in the Eulerian location  $x(q_s)$ . Overall, the eigenvalue condition  $1 + \mu_i = 0$  defines a two-dimensional sheet in Lagrangian space. This sheet forms a singularity, containing points  $q$  that function as singularity points. If, however, both  $1 + \mu_1 = 0$  and  $1 + \mu_2 = 0$ , then  $T$  will be a vector orthogonal to the eigenvector  $v_3$ . The eigenvalue conditions define a line through three-dimensional Lagrangian space, the points  $q$  along which are singularity points. Conversely, if  $1 + \mu_i \neq 0$  for all  $i$ , then there does not exist a  $T$  satisfying the general shell-crossing condition.

### 3.4 Shell-crossing conditions: coordinate transformation

The shell-crossing conditions are manifestly independent of coordinate choices. However, the eigenvalue and eigenvector fields generally do depend on the choice of coordinates. By themselves, they do therefore not provide valid descriptions of the dynamics of the fluid. Suppose the displacement field can be written as  $s = \nabla\psi$  for some potential  $\psi$ . The Hessian  $H_x$  of  $\psi$ ,

$$H_{ij} = \frac{\partial^2 \psi}{\partial x_i \partial x_j}, \quad (3.15)$$

transforms non-trivially under the local coordinate transformation  $x \rightarrow X(x)$  i.e.

$$H \rightarrow \tilde{H} = J^T H J + J^T \nabla(J) \nabla\psi, \quad (3.16)$$

---

<sup>5</sup> $T_{q_s}M$  is the vector space of all tangential vectors to the manifold  $M$  in  $q_s \in M$ .

with  $J$  the Jacobian between the coordinate systems  $X$  and  $x$ ,

$$J_{ij} = \frac{\partial X_i}{\partial x_j}. \quad (3.17)$$

From this we immediately infer that the eigenvalue field and eigenvector fields are invariant if the transformation is orthogonal and global, i.e. if  $J^T = J^{-1}$  and  $\nabla(J) = 0$ . As may be expected, these transformations include rotations and translations.

## 4 Caustic conditions

In section 3, we inferred the general condition for shell-crossing. The condition establishes the relation between the eigenvalue and eigenvector fields of the deformation tensor in Lagrangian space, and the Lagrangian regions that get incorporated in features of infinite density in Eulerian space. Moreover, it allows us to establish the identity of the resulting singularity in Eulerian space. The stable singularities that may emerge in generic fluids or in Hamiltonian fluids, can be classified in two series, the  $A_k$  and  $D_k$  series<sup>6</sup>. The shell-crossing conditions state that a necessary and sufficient condition for the generation of caustics is that  $1 + \mu_i = 0$  for at least one  $i$ . The  $A$ -family of caustics are the ones for which this condition holds for only one eigenvalue. Caustics for which two eigenvalues simultaneously satisfy this condition belong to the  $D$ -family. In three-dimensional fluids, the case in which all eigenvalues simultaneously satisfy this condition is non-degenerate. They belong to the  $E$ -family. However, we will not discuss them in the context of the present paper. In section 5, we will describe these series of caustics in more detail.

While already using the terminology of the  $A_k$  and  $D_k$  classification of singularities, the purpose of the caustic conditions inferred in this section is precisely to establish the foundation on which to base this classification. Along with a detailed description of the classification, this will be the task of next section 5 by connecting the caustic conditions to the classification of stable singularities.

In this section we restrict ourselves to the three-dimensional situation. Within 3-D space we seek to identify and quantify the Lagrangian regions that get folded into  $A_k$  or  $D_k$  singularities. As one may readily infer from the shell-crossing conditions, this is determined by the spatial characteristics of the deformation tensor eigenvalue and eigenvector fields in Lagrangian space. The conditions that are inferred from this analysis for caustics in Lagrangian fluids are called the *caustic conditions*.

With the purpose to provide a guide that evokes a visual intuition for the connection between the structure and geometry of the eigenvalue fields and the formation of the various singularities, in particular those of the  $A$ -family, we include figure 4. It shows a contour map representing the typical structure of the eigenvalue field  $\mu_i$ . This field corresponds to a two-dimensional Gaussian random density field. For reasons of convenience, we have assumed higher eigenvalues to correspond to earlier collapse, and negative ones to no collapse (in other words, we have mirrored  $\mu_i$ ). The geometry and topology of the eigenvalue landscape is decisive for the occurrence of singularities. This may already be inferred from the positions of different  $A$ -family singularity points and varieties, whose positions are indicated on the contour map.

---

<sup>6</sup>The classification ultimately has its origin in the classification of Coxeter groups

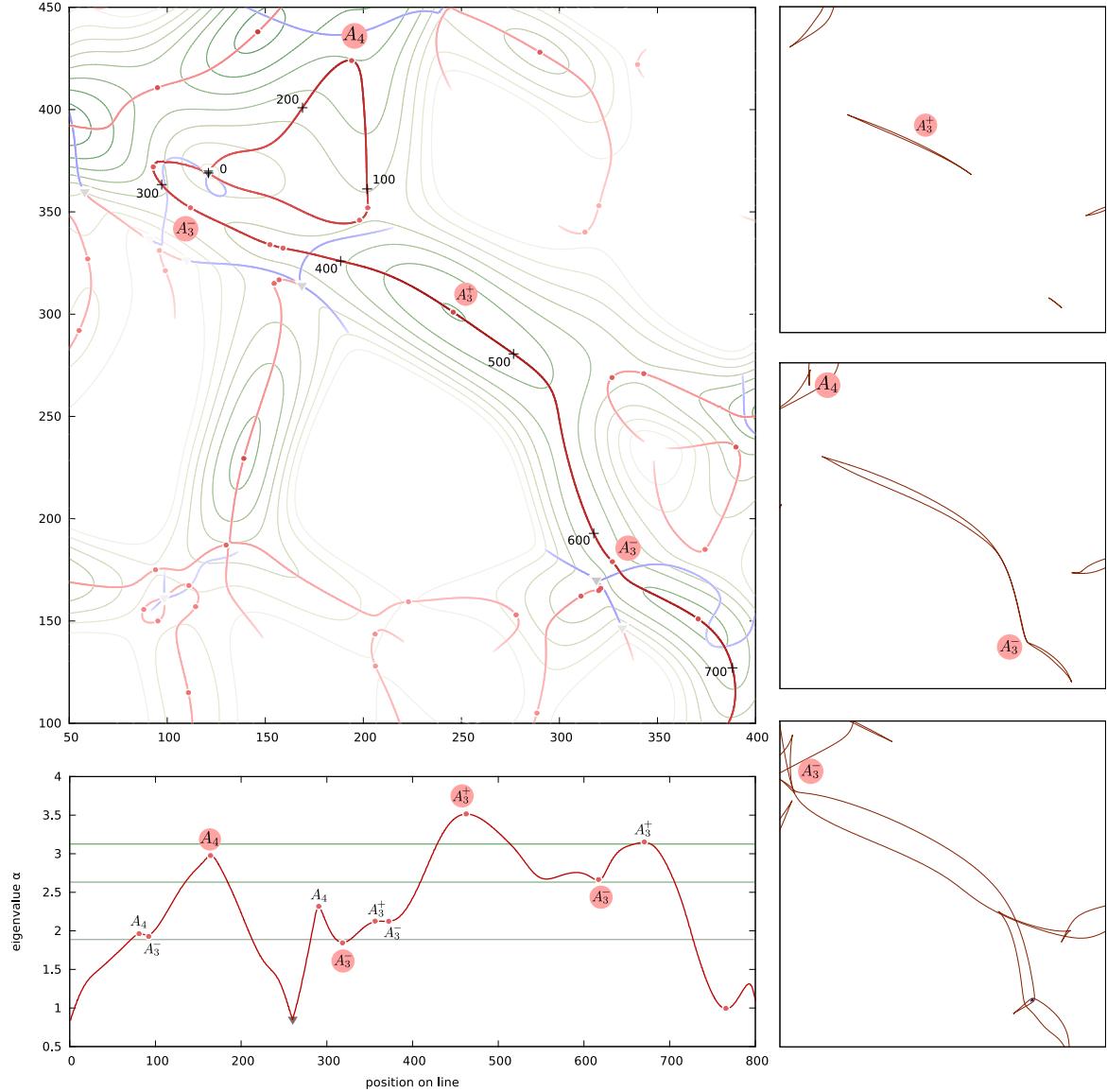


**Figure 4:** Eigenvalue field and singularity points. Top lefthand frame: the contour map illustrates the typical structure of the eigenvalue field corresponding to a 2-D Gaussian random density field. Indicated are the positions of different  $A$ -family singularity points and varieties. In particular noteworthy is the run of the  $A_3$  line, which defines the ridge along which we may identify a range of  $A$  singularities. One may keenly appreciate how the identity of the various singularities is determined by the specific geometric character of the eigenvalue field  $\mu(q)$ , as expressed in its gradient  $\nabla\mu(q)$  and higher order gradients. Bottom lefthand frame: the panel depicts the run of the eigenvalue field along the  $A_3$  curve (in the contour map of top lefthand frame). Note the location of the  $A_3^\pm$  points and  $A_4$  points on the extrema of the curve. Righthand panels: the three panels show the evolution, in Eulerian space, of the  $A_3$  line, according to the linear Lagrangian Zel'dovich approximation (Zel'dovich 1970). Note the appearance of the corresponding caustics and the relation between the geometry of the  $A_3$  line in Eulerian space and the  $A_3^\pm$  and  $A_4$  points.

The landscape defined by the eigenvalue contours is varied, characterized by several peaks, connected by ridges with lower  $\mu_i$  values. These, in turn, are connected to valleys in which  $\mu_i$  attains negative values that will prevent collapse – along the direction of the eigenvector  $v_i$  – of the corresponding mass elements at any time. From the density relation (eqn. (2.6)), we know that the region of space that has undergone collapse before the current epoch (i.e. attained an infinite density) is the superlevel set of the eigenvalue field defined by the current value  $\mu_{ti}$ . For each time  $t$ , the positive value contours correspond to the  $A_2(t)$  fold sheets. Collapse occurs first at the maxima in the field. These mark the birth of new features, and are designated by the label of  $A_3^+$  points. Evidently, the steepness of the hill around these maxima, i.e. the gradient  $\nabla\mu_i(q)$ , will determine how and which mass elements around the hill will follow in outlining the emerging feature around the  $A_3^+$  points.

In particular noteworthy is the run of the  $A_3$  line. The key significance of the  $A_3$  curve is evident from the observation that all  $A$ -family singularities are aligned along the ridge. In two-dimensional space, the  $A_3$  curves delineate the points where the eigenvalues  $\mu_i$  are maximal along the direction of the corresponding local eigenvector. At these points, along the eigenvector direction, the gradient of the eigenvalues is zero, i.e. they are the points where the eigenvector  $n$  is perpendicular to the local gradient of  $\nabla\mu_i$  of the eigenvalue field. Below, in section 4.1.3, we will see that this follows directly from the shell-crossing conditions that were derived in the previous section. Because of this there is a line-up and accumulation of neighbouring mass elements that simultaneously pass through the singularity. When mapped to Eulerian space, this evokes the formation of an  $A_3$  cusp.

To illustrate the connection between  $A_3$  curves and the various singularities even more strongly, the bottom lefthand panel depicts the run of the eigenvalue field along the  $A_3$  curve. In particular noteworthy is the location of the  $A_3^\pm$  points and  $A_4$  points on the extrema of the curve. A prominent aspect of this is the presence of the  $A_3^-$  points at saddle junctions in the eigenvalue field. These are topologically the most interesting locations, as they evoke the merging of separate fold sheets into a single structure. In other words, they are the points where the topological structure of the field undergoes a transition and where the connectivity of the emerging structural features is established. To establish this even more strongly, the three righthand panels of figure 4 represent a time sequence of the evolving structure along the  $A_3$  line as it is mapped to its appearance in Eulerian space. The evolution follows the linear Lagrangian Zel'dovich approximation (see [73] and appendix A). We may note the appearance and merging of the corresponding caustics.

In all, one may keenly appreciate how the identity of the various singularities is determined by the specific geometric character of the eigenvalue field  $\mu_i(q)$ , as expressed in its gradient  $\nabla\mu_i(q)$  and higher order gradients. In the following subsections, we will systematically inventorize the families of singularities on the basis of the shell-crossing conditions that we inferred before, and observe the connection between the singularities and the geometry of the eigenvalue field.

## 4.1 The $A$ family

The  $A$  family of caustics form when

$$\begin{aligned} 1 + \mu_i &= 0, \\ 1 + \mu_k &\neq 0 \quad \text{for } k \neq i, \end{aligned} \tag{4.1}$$

for some  $i$ . In other words, the caustics correspond to one eigenvalue field. In this case, the eigenvector fields  $\{v_i\}$  and their dual vector fields  $\{v_i^*\}$  are linearly independent. In addition,

we may assume the eigenvalue fields to be sufficiently differentiable.

In total, we may identify 5 different  $A$  classes. These run from the trivial  $A_1$  class, corresponding to the points that never form caustics, to the highest dimensional  $A$  singularity class, the  $A_5$  butterfly caustics. The  $A$  family includes the sheetlike  $A_2$  fold singularities, the curvelike  $A_3$  cusp singularities, the  $A_4$  swallowtail singularities and the  $A_5$  butterfly singularity.

#### 4.1.1 The trivial $A_1$ class

The  $A_1$  class labels the points which never form caustics.

According to the shell-crossing condition,  $q_s$  will form a singularity at time  $t$  if and only if there exists a nonzero tangent vector  $T \in T_{q_s}L$  for which

$$(1 + \mu_i(q_s))v_i^*(q_s) \cdot T = 0 \quad (4.2)$$

for all  $i$ . The point  $q_s$  will not satisfy this condition if  $1 + \mu_i(q_s) \neq 0$  for all  $i$  since the three dual vectors  $\{v_i^*\}$  span the tangent space  $T_{q_s}L$ .

From the shell-crossing condition we therefore conclude that the three-dimensional variety  $A_1$ ,

$$A_1 = \{q \in L \mid 1 + \mu_{ti}(q) \neq 0 \text{ for all } i \text{ and } t\}, \quad (4.3)$$

consists of the points never forming caustics. In this respect we should note that the displacement map at the initial time is the zero map, so that the eigenvalues at the initial time are equal to zero, i.e.  $\mu_{0i}(q) = 0$  for all  $q \in L$ . Since the eigenvalues are continuous function of time, the requirement for a point  $q$  to belong to  $A_1$  is equivalent to  $\mu_{ti}(q) > -1$ .

#### 4.1.2 The $A_2$ caustics

Based on the discussion above, we may conclude that for a given  $i$ ,  $i = 1 \dots 3$ , at time  $t$  the points

$$A_2^i(t) = \{q \in L \mid 1 + \mu_{ti}(q) = 0\} \quad (4.4)$$

form a singularity. For three-dimensional fluids, the set  $A_2(t)$  forms a two-dimensional sheet, sweeping through space as the fluid evolves. These singularities can be associated to the  $A_2$  fold singularity class.

From this, we conclude that the set of points which form a  $A_2$  fold singularity at a time  $t \in [0, \infty)$  is given by

$$A_2^i = \{q \in L \mid 1 + \mu_{ti}(q) = 0 \text{ for some } t\}. \quad (4.5)$$

#### 4.1.3 The $A_3$ caustics

Following up on the folding of the fluid to the  $A_2^i$  singularity, the  $A_2^i$  manifold itself may actually be folded into a more complex configuration. The result is a so-called  $A_3$  singularity. To guide understanding in the emergence of cusps we may refer to the eigenvalue contour map of figure 5.

To infer the identity of the  $A_3^i$  caustic, we restrict the criterion for shell-crossing to points on the  $A_2^i$  manifold. In other words, we look for points  $q_s$  on the surface of the sheetlike variety  $A_2^i(t)$  that fulfill the criterion for shell-crossing.

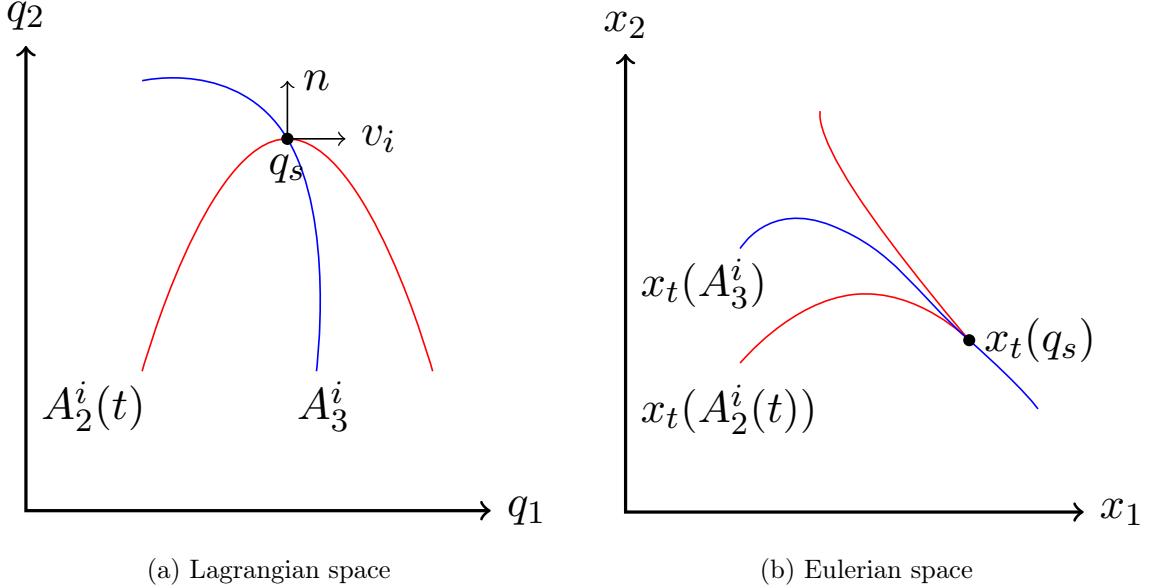


**Figure 5:** The formation of a cusp ( $A_3$ ) singularity in a Lagrangian map  $x_t$ . The left panel shows Lagrangian space, describing the initial positions of the fluid. The right panel shows Eulerian space, describing the positions of the fluid at time  $t$ . The fluid undergoes shell-crossing along the fold  $A_2^i(t)$  (red) at time  $t$ . The fold gets mapped under the Lagrangian map to  $x_t(A_2)$  (red), which is folded into a cusp in the point  $x_t(q_s)$  corresponding to  $q_s$ . The cusp forms if and only if the normal  $n$  of  $A_2^i(t)$  is orthogonal to the eigenvector field  $v_i$  in  $q_s$ . Over time, the cusp traces out the curve  $A_3^i$  (blue) which is mapped to  $x_t(A_3^i)$  (blue).

A point  $q_s \in A_2^i(t)$  forms a singularity if there exists a nonzero tangent vector  $T$ ,  $T \in T_{q_s} A_2^i(t)$ , orthogonal to the span $\{v_j^* | j \neq i\}$ . This condition is satisfied if and only if the tangent vector  $T$  is parallel to  $v_i$ . This is equivalent to the condition that  $v_i$  is orthogonal to the normal  $n = \nabla \mu_{ti}$  of the manifold  $A_2^i(t)$  in the point  $q_s$ . Explicitly, this means that the inner product of  $n$  with  $v_i$  is equal to 0,

$$\mu_{ti,i} \equiv v_i \cdot \nabla \mu_{ti} = 0. \quad (4.6)$$

The points  $q$  forming a cusp at time  $t$  therefore represent the one-dimensional variety defined by

$$A_3^i(t) = \{q \in L | q \in A_2^i(t) \wedge \mu_{ti,i}(q) = 0\}. \quad (4.7)$$

Extrapolating this to the set of all points  $q$  that at some time  $t \in [0, \infty)$  have belonged to or will be incorporated in a cusp singularity defines a two-dimensional variety

$$A_3^i = \{q \in L | q \in A_2^i(t) \wedge \mu_{ti,i}(q) = 0 \text{ for some } t\}, \quad (4.8)$$

which is the assembly of all  $A_3^i(t)$  over the time interval  $t \in [0, \infty)$ .

#### 4.1.4 The $A_3^\pm$ points

The topology of the sheetlike  $A_2^i(t)$  variety changes as a function of time. These topological changes occur at critical points of the corresponding eigenvalue field  $\mu_{ti}$ . It is at these points

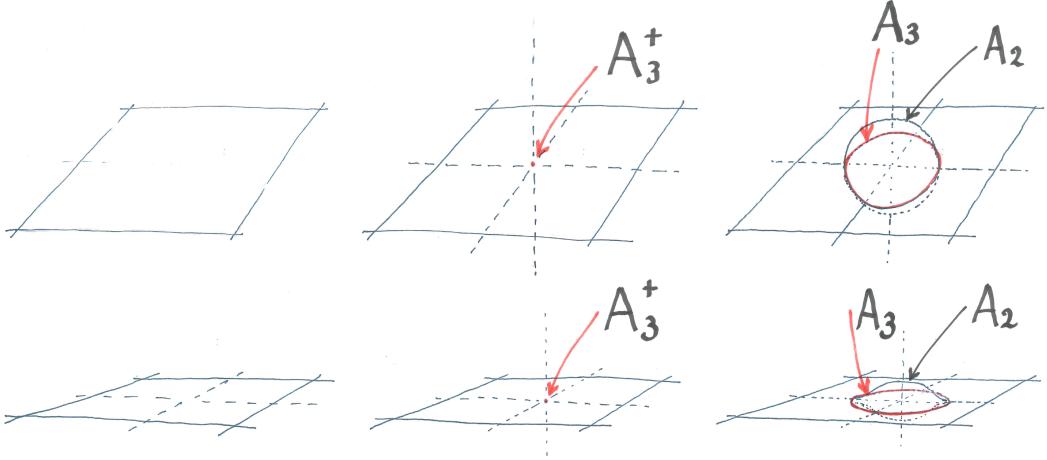


**Figure 6:** The creation/annihilation of a fold ( $A_2$ ) sheet in a  $A_3^+$  point. The upper three panels show the unfolding of a  $A_3^+$  singularity in Lagrangian space. The lower three panels show the corresponding unfolding in Eulerian space. The two panels on the left show the cusp ( $A_3$ ) plane on which the cusps form. The middle panels show the appearance of a  $A_3^+$  singularity in which a fold sheet is formed/removed. The right panels show the resulting fold ( $A_2$ ) sheet. The fold sheet gets folded into a cusp ( $A_3$ ) curve (red). This configuration is known as the *Zel'dovich pancake* (Zel'dovich 1970).

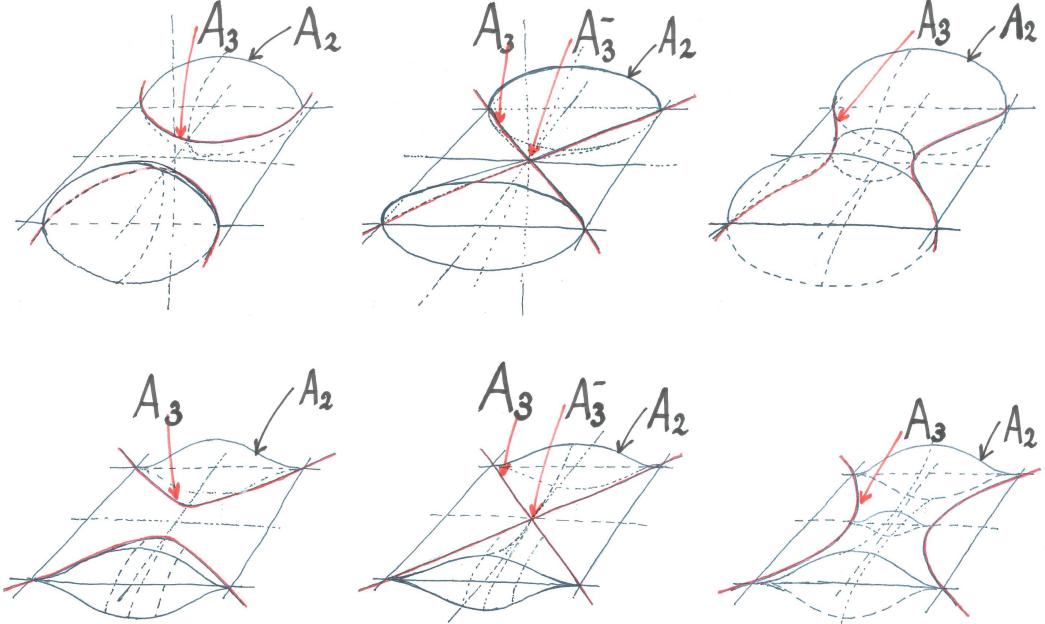


**Figure 7:** The merger/splitting of a fold ( $A_2$ ) sheet in a  $A_3^-$  point. The upper three panels show the unfolding of a  $A_3^-$  singularity in Lagrangian space. The lower three panels show the corresponding unfolding in Eulerian space. The two panels on the left show two fold ( $A_2$ ) sheets, two cusp ( $A_3$ ) curves (red) and the cusp ( $A_3$ ) plane on which the cusps form. The middle panels show the merger/splitting of the two fold ( $A_2$ ) sheets in a  $A_3^-$  singularity. The right panels show the resulting merged fold ( $A_2$ ) sheet. This configuration is known as the *Kissing Lips*.

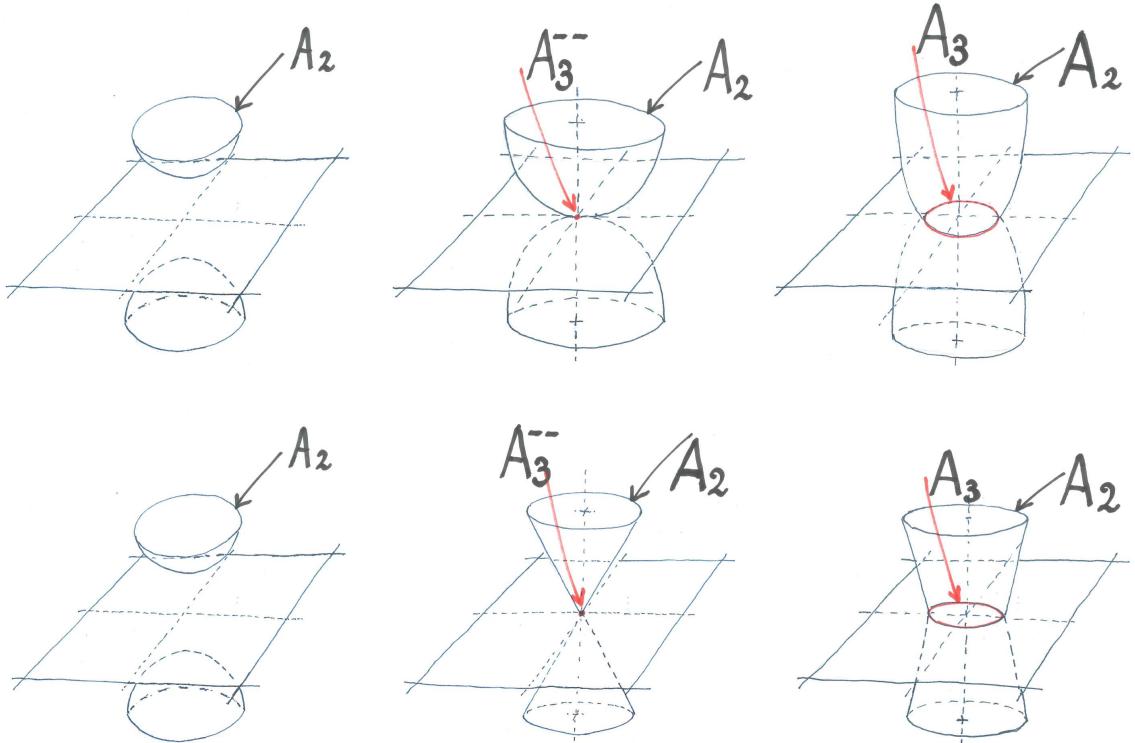


**Figure 8:** The merger/splitting of a fold ( $A_2$ ) sheet in a  $A_3^{--}$  point. The upper three panels show the unfolding of a  $A_3^{--}$  singularity in Lagrangian space. The lower three panels show the corresponding unfolding in Eulerian space. The two panels on the left show two fold ( $A_2$ ) sheets, and the cusp ( $A_3$ ) plane on which the cusps form. The middle panels show the merger/splitting of the two fold ( $A_2$ ) sheets in a  $A_3^{--}$  singularity. The right panels show the resulting merged fold ( $A_2$ ) sheet with the corresponding cusp ( $A_3$ ) curve.

where in Eulerian space we see the emergence of new features, the disappearance of features and/or the merging of features. The critical points are classified as cusp singularities.

At minima of the  $\mu_i$  field, a feature gets created. At maxima, a feature gets annihilated. Particularly interesting points are the saddle points. In three-dimensional space, there are two classes of saddles in the eigenvalue field  $\mu_{ti}$ . The index 1 saddles have a Hessian signature  $(- - +)$ , with 1 positive eigenvalue, while the index 2 saddles have a signature  $(- + +)$ .

Based on their impact on caustic structure, Arnol'd used a slightly different classification scheme, in which he distinguished between  $A_3^{++}$ ,  $A_3^{+-}$  and  $A_3^{--}$  points [8]. The  $A_3^{++}$  points are identified with the minima<sup>7</sup>, while the  $A_3^{+-}$  points are the saddle points for which the  $A_3$  sheet intersects the two disjoint  $A_2$  sheets. This is illustrated in the upper left panel in figure 7. The additional  $A_3^{--}$  points correspond to saddle points for which the  $A_3$  sheet does not intersect the disjoint  $A_2$  sheets. Because this concerns a non-generic situation, we do not treat it here. Also note that higher dimensional fluids will have additional  $A_3$  points.

In the context of this paper we therefore use a slightly shorter notation for the maxima,

---

<sup>7</sup>Note that in Arnol'd's notation, related to the Zel'dovich formalism (see appendix A), these are the maxima of the eigenvalue field

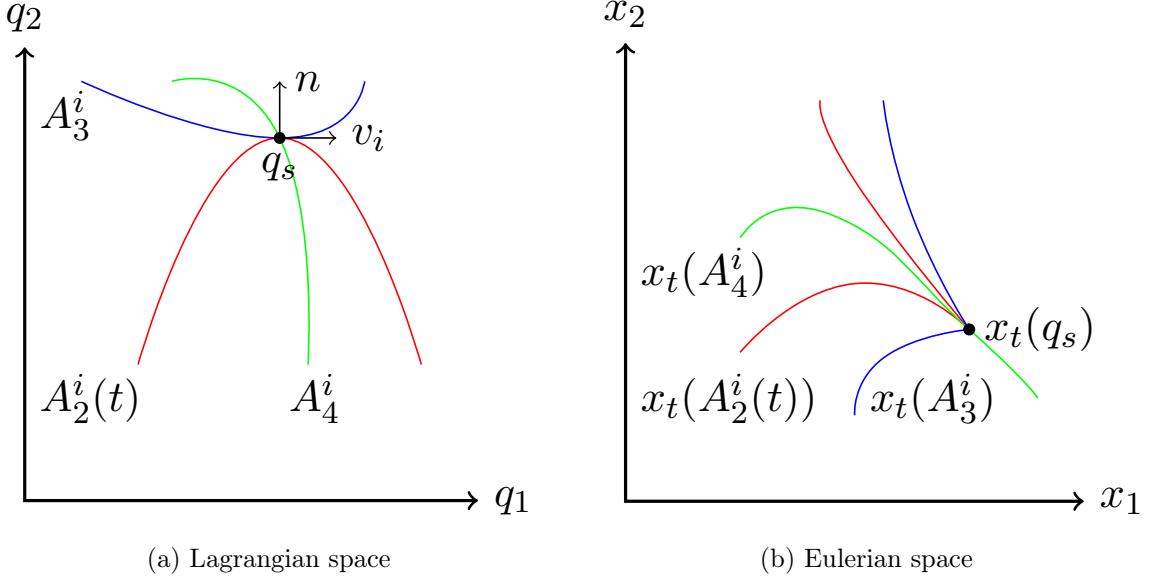


**Figure 9:** The formation of a swallowtail ( $A_4$ ) singularity in a Lagrangian map  $x_t$ . The left panel shows the Lagrangian space describing the initial positions of the fluid. The right panel shows the Eulerian space describing the positions of the fluid at time  $t$ . The fluid undergoes shell-crossing along  $A_2^i(t)$  (red) at time  $t$ . The fold gets mapped in Eulerian space, under the Lagrangian map, to  $x_t(A_2)$  (red), which is folded into a cusp in the point  $x_t(q_s)$  corresponding to  $q_s$ . The cusp forms if and only if the normal  $n$  of  $A_2^i(t)$  is orthogonal to the eigenvector field  $v_i$  in  $q_s$ . Over time, in Lagrangian space the cusp traces out the curve  $A_i$  (blue) which in Eulerian space is mapped to  $x_t(A_3^i)$  (blue). Since the cusp ( $A_3^i$ ) curve is tangential to the fold ( $A_2$ ) curve in  $q_s$ , the cusp curve  $x_t(A_3^i)$  forms a swallowtail ( $A_4$ ) singularity. Over time, the swallowtail traces out  $A_4^i$  (green), which in Eulerian space is mapped into  $x_t(A_4^i)$  (green).

minima and saddles, classifying them as the cusp singularities  $A_3^+$  and  $A_3^-$ ,

$$\begin{aligned} A_3^{i+} &= \{q \in L | q \in A_2^i(t) \wedge \mu_{ti}(q) \text{ max-/minimum of } \mu_{ti} \text{ at some time } t\}, \\ A_3^{i-} &= \{q \in L | q \in A_2^i(t) \wedge q \text{ saddle point of } \mu_{ti} \text{ at some time } t\}. \end{aligned} \quad (4.9)$$

Note that in this scheme, the saddle points with index 1 and 2 belong to the same singularity class  $A_3^{i-}$ . For an illustration of the  $A_3^+$  and  $A_3^-$  singularities, we refer to figures 6 and 7. From the caustics conditions we may directly infer that the  $A_3^{i\pm}$  points are located on the  $A_3^i$  variety.

#### 4.1.5 The $A_4$ caustics

In Eulerian space the  $A_3^i(t)$  variety gets folded in points associated with  $A_4$  swallowtail singularities.

The identity of the points defining the variety  $A_4^i(t)$  can be inferred by the application of the general shell-crossing condition (eqn. (3.14)) to the point set defining the  $A_3^i(t)$  variety (see figure 9). On the basis of this, the  $A_4^i$  identity is defined as

$$A_4^i(t) = \{q \in L | q \in A_3^i(t) \wedge \mu_{ti,ii}(q) = 0\}, \quad (4.10)$$

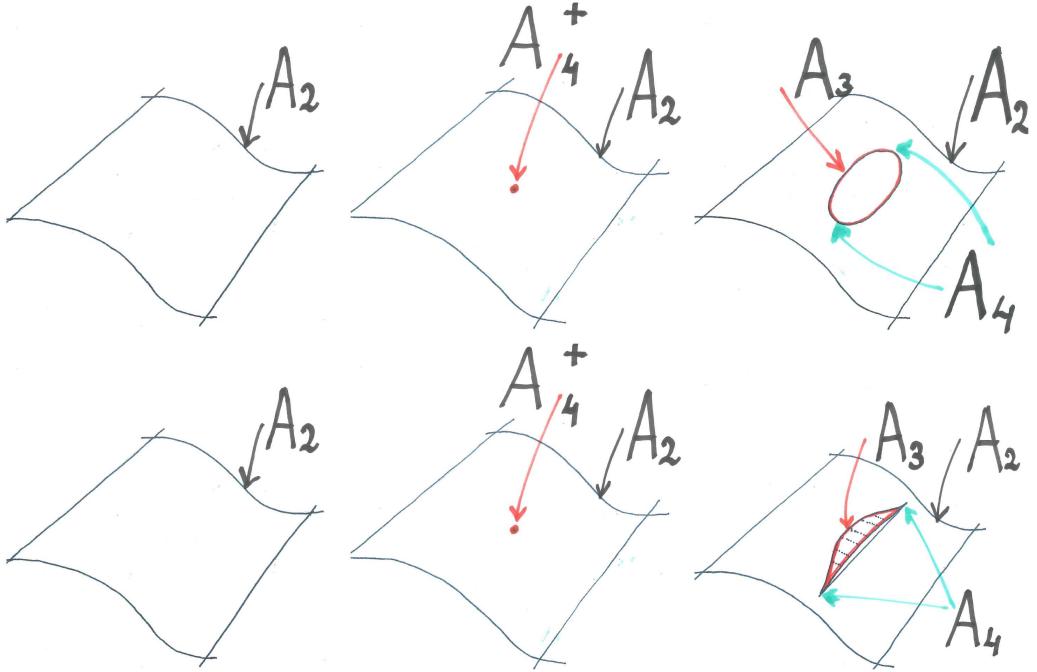


**Figure 10:** The creation/annihilation of a swallowtail ( $A_4$ ) singularity in a  $A_4^+$  point. The upper three panels show the unfolding of a  $A_4^+$  singularity in Lagrangian space. The lower three panels show the corresponding unfolding in Eulerian space. The two panels on the left show a fold ( $A_2$ ) sheet. The middle panels show a  $A_4^+$  point on the fold ( $A_2$ ) sheet. The  $A_4^+$  point leads to the creation/annihilation of two swallowtail ( $A_4$ ) singularities. The right panels show the resulting cusp ( $A_3$ ) curves and swallowtail ( $A_4$ ) singularities.

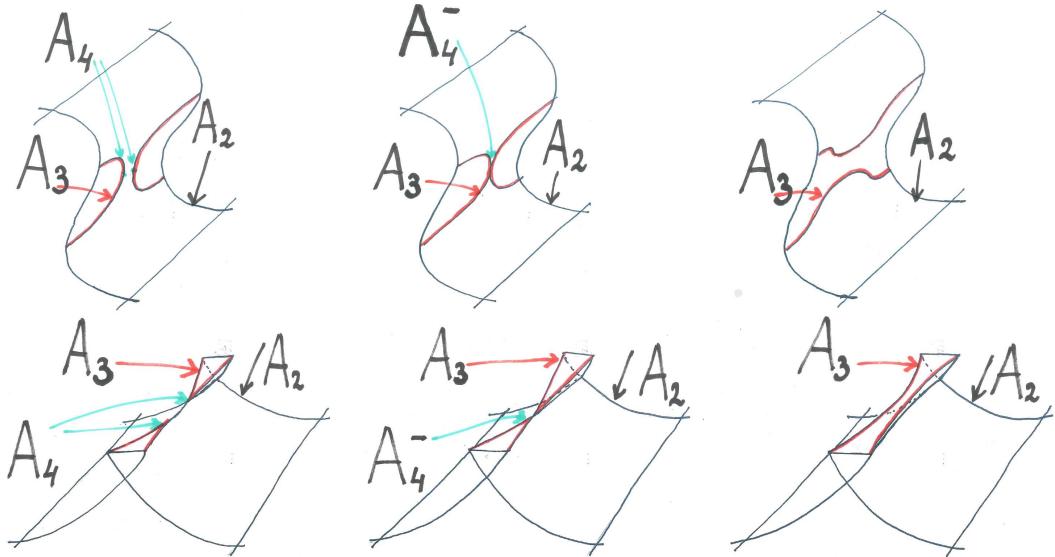


**Figure 11:** The merger/splitting of a cusp ( $A_3$ ) curve in a  $A_4^-$  point. The upper three panels show the unfolding of a  $A_4^-$  singularity in Lagrangian space. The lower three panels show the corresponding unfolding in Eulerian space. The two panels on the left show a fold ( $A_2$ ) sheet, cusp ( $A_3$ ) curves and swallowtail ( $A_4$ ) singularities. The middle panels show the merger/splitting of the cusp ( $A_3$ ) curves in a  $A_4^-$  point. The right panels show the resulting fold ( $A_2$ ) sheet and cusp ( $A_3$ ) curves singularities.

with  $\mu_{ti,ii}(q)$  the inner product of the normal  $n = \nabla\mu_{ti,i}$  with the eigenvector  $v_i$ ,

$$\mu_{ti,ii} \equiv v_i \cdot \nabla\mu_{ti,i}. \quad (4.11)$$

Integrated over time, the points on the varieties  $A_3^i(t)$  trace out the 1-dimensional variety  $A_4^i$ , i.e. the 1D line  $A_4^i$  is the set of all points  $A_3^i(t)$  over the time interval  $t \in [0, \infty)$ ,

$$A_4^i = \{q \in L | q \in A_3^i(t) \wedge \mu_{ti,ii}(q) = 0 \text{ for some } t\}. \quad (4.12)$$

#### 4.1.6 The $A_4^\pm$ points

Also the topology of the variety  $A_3^i(t)$  changes as a function of time. To this end, we identify the critical points of the field  $\mu_{ti,i}$ ,

$$\mu_{ti,i} \equiv v_i \cdot \nabla\mu_{ti}. \quad (4.13)$$

Constraining the location of these singularities to the one-dimensional curvelike variety  $A_3^i(t)$ , and thus implicitly also to the two-dimensional membrane of the variety  $A_2^i(t)$ , these  $A_4^\pm$  points mark the locations at which topological changes occur. They represent the sites at which we see the birth of new singularities in Eulerian space, or the annihilation of and/or merging of such features. These singularities are classified as swallowtail singularities.

The birth or death of features on  $A_3^i(t)$  takes place at maxima and minima of  $\mu_{ti,i}$ , and is identified with  $A_4^{i+}$  singularities. The merging or splitting of features happens at the saddle points of the same field  $\mu_{ti,i}$ . The latter mark the  $A_4^{i-}$  singularities,

$$\begin{aligned} A_4^{i+} &= \{q \in L | q \in A_3^i(t), \mu_{ti,i}(q) \text{ max-/minimum of } \mu_{ti,i}|_{A_2^i(t)} \text{ for some } t\}, \\ A_4^{i-} &= \{q \in L | q \in A_3^i(t) \text{ saddle point of } \mu_{ti,i}|_{A_2^i(t)} \text{ for some } t\}. \end{aligned} \quad (4.14)$$

The  $A_4^\pm$  critical points are constrained to lie on the curvelike variety  $A_2^i(t)$ . Their identity is therefore determined by the interplay between the geometric properties of two entities. One of these is the geometry of the field  $\mu_{ti,i}$ , the other that of the geometry of the curvelike variety  $A_2^i(t)$ . For illustrations of the  $A_4^+$  and  $A_4^-$  singularities we refer to figure 10 and 11.

From the caustic conditions – as expressed in eqn. (4.10) – we may also immediately observe that the  $A_4^\pm$  points belong to the  $A_4^i$  variety. In fact, this also represents a condition on the topology of the field  $\mu_{ti,i}$  and that of the  $A_2^i(t)$  variety.

#### 4.1.7 The $A_5$ caustics

Finally, also the swallowtail curves  $A_4^i$  curve get folded in Eulerian space. It leads to the emergence of so-called butterfly singularities, or  $A_5$  singularities. Following the same reasoning as for the  $A_3^i$  and  $A_4^i$  varieties, we may infer from the general shell-crossing condition that the  $A_4^i$  curve gets folded in the points,

$$A_5^i = \{q \in L | q \in A_4^i(t) \text{ and } \mu_{ti,iii} = 0 \text{ for some time } t\}. \quad (4.15)$$

Figure 12 shows an illustration of a  $A_5$  singularity.

The butterfly singularity is the highest dimensional singularity that may surface in three-dimensional Lagrangian fluids. It is important to realize that the butterfly singularity only exists at one point in space-time.

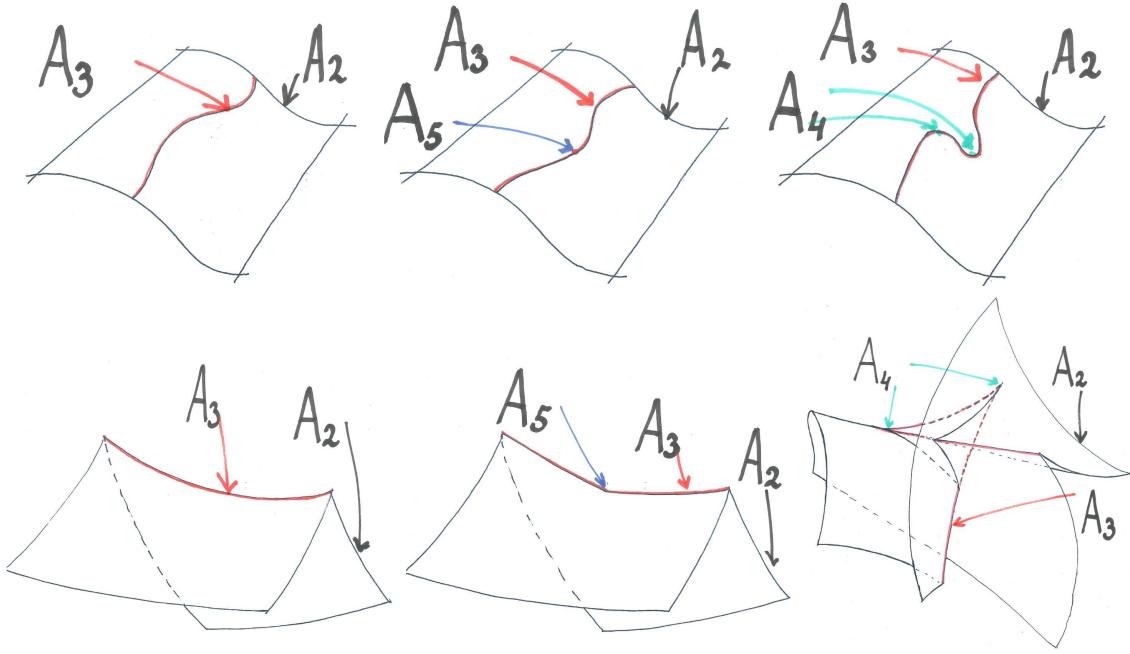


**Figure 12:** The creation/annihilation of swallowtail singularities in a butterfly ( $A_5$ ) singularity. The upper three panels show the unfolding of a  $A_5$  singularity in Lagrangian space. The lower three panels show the corresponding unfolding in Eulerian space. The two panels on the left show a fold ( $A_2$ ) sheet, and cusp ( $A_3$ ) curve. The middle panels show the creation/annihilation of the butterfly ( $A_5$ ) singularity on the cusp ( $A_3$ ) curve. The right panels show the resulting fold ( $A_2$ ) sheet, cusp ( $A_3$ ) curve and swallowtail ( $A_4$ ) singularities.

## 4.2 The $D$ family

The  $D$  family of caustics correspond to manifolds for which the caustic conditions holds for two eigenvalue fields simultaneously,

$$\begin{aligned} 1 + \mu_i &= 0, \\ 1 + \mu_j &= 0, \quad \text{for } j \neq i \\ 1 + \mu_k &\neq 0, \quad \text{for } k \neq i, j. \end{aligned} \tag{4.16}$$

From this, we may immediately infer that these caustics form at the intersection of two  $A_2(t)$  fold sheets, the  $A_2^i(t)$  and  $A_2^j(t)$  varieties. In all, two families of  $D$  caustics can be identified, the  $D_4$  elliptic and hyperbolic umbilic caustics and the  $D_5$  parabolic umbilic caustic.

### 4.2.1 The $D_4$ caustics

The  $D_4$  caustics are defined by the points  $q$  in Lagrangian space, at which two of the eigenvalues have the same value. For instance, the  $D_4^{ij}(t)$  caustic, with  $i \neq j$ , is outlined by the points  $q$  for which at the time  $t$  the eigenvalues  $\mu_i(t)$  and  $\mu_j(t)$  are equal,  $\mu_{ti} = \mu_{tj}$ . While the eigenvalue  $\mu_{ti}$  defines the fold sheet  $A_2^i$ , and the eigenvalue  $\mu_{tj}$  the fold sheet  $A_2^j$ , the umbilic  $D_4^{ij}$  caustic consist of the set of points  $q$  for which

$$D_4^{ij}(t) = \{q \in L | q \in A_2^i(t) \cap A_2^j(t)\}. \tag{4.17}$$

In three-dimensional space, one would expect that the intersection of the two sheets  $A_2^i(t)$  and  $A_2^j(t)$  to consist of one-dimensional curves. This would certainly be true for two sheets that would be entirely independent of each other. However, the situation at hand concerns a highly constrained situation, in which the two eigenvalues  $\mu_i$  and  $\mu_j$  are strongly correlated.

Because of the latter, the intersection between the folds  $A_2^i$  and  $A_2^j$  is considerably more complex. Instead of a continuous curve, the intersection consists of isolated, singular points. A telling illustration – and discussion – of this, for the two-dimensional situation, can be found in [39].

### The $D_4$ equation

To investigate the geometry and structure of the set  $D_4^{ij}(t)$  we focus on the particular situation of the set  $D_4^{12}(t)$ , in which the two first eigenvalues  $\mu_1$  and  $\mu_2$  have the same value,  $\mu_{t1} = \mu_{t2}$ . Without loss of generality, we transform the coordinate system such that the third eigenvector  $v_3$  defines the  $q_3$  axis. This transformation makes the  $q_1 q_2$ -plane the one in which we see the folding and collapse of the phase space sheets to the  $A_2^1$  and  $A_2^2$  caustics. In this coordinate system, the deformation tensor  $\mathcal{M}$  has the form

$$\mathcal{M} = \begin{pmatrix} M_{11} & M_{12} & 0 \\ M_{12} & M_{22} & 0 \\ 0 & 0 & \mu_3 \end{pmatrix}, \quad (4.18)$$

in which  $\mu_3$  is the third eigenvalue of  $\mathcal{M}$ . The eigenvalues  $\mu_1$ ,  $\mu_2$  and  $\mu_3$  are obtained from the resulting characteristics polynomial,

$$\begin{aligned} \chi(\mu) &= \mathcal{M} - \mu I \\ &= [\mu^2 - \text{Tr}(\tilde{\mathcal{M}})\mu + \det(\tilde{\mathcal{M}})](\mu_3 - \mu) = 0, \end{aligned} \quad (4.19)$$

in which the  $\tilde{\mathcal{M}}$  is the  $\{12\}$ -submatrix of the deformation tensor,

$$\tilde{\mathcal{M}} = \begin{pmatrix} M_{11} & M_{12} \\ M_{12} & M_{22} \end{pmatrix}, \quad (4.20)$$

with trace  $\text{Tr}(\tilde{\mathcal{M}})$  and determinant  $\det(\tilde{\mathcal{M}})$ ,

$$\begin{aligned} \text{Tr}(\tilde{\mathcal{M}}) &= M_{11} + M_{22}, \\ \det(\tilde{\mathcal{M}}) &= M_{11}M_{22} - M_{12}^2. \end{aligned} \quad (4.21)$$

Solving the characteristic polynomial equation yields for the first two eigenvalues  $\mu_1$  and  $\mu_2$ ,

$$\mu_{1,2} = \frac{1}{2} \left( \text{Tr}(\tilde{\mathcal{M}}) \pm \sqrt{\text{Tr}(\tilde{\mathcal{M}})^2 - 4 \det(\tilde{\mathcal{M}})} \right), \quad (4.22)$$

while, evidently, the third eigenvalue is  $\mu_3$ . For the particular situation of the  $D_4^{12}$  caustic, we know that  $1 + \mu_1 = 1 + \mu_2 = 0$ , and hence that  $\mu_1 = \mu_2 = \mu$  (see eqn. (4.16)). This translates into the condition that

$$\text{Tr}(\tilde{\mathcal{M}})^2 = 4 \det \tilde{\mathcal{M}}. \quad (4.23)$$

Expressed in terms of the  $\tilde{\mathcal{M}}$  matrix elements, this condition translates into

$$(M_{11} - M_{22})^2 + 4M_{12}^2 = 0, \quad (4.24)$$

from which we obtain the following 2 conditions for the  $D_4^{12}$  caustic.

$$\begin{aligned} M_{11}(q) &= M_{22}(q), \\ M_{12}(q) &= 0. \end{aligned} \quad (4.25)$$

These two conditions immediately imply that the matrix  $\tilde{\mathcal{M}}$  is proportional to the identity matrix,

$$\tilde{\mathcal{M}} = \begin{pmatrix} \mu & 0 \\ 0 & \mu \end{pmatrix}. \quad (4.26)$$

#### *$D_4$ singularities and $A_3$ varieties*

An additional important consequence of the inferred constraints (4.25) for the  $D_4$  singularities is that  $D_4^{ij}$  points will always be located on the two corresponding  $A_3$  varieties,  $A_3^i$  and  $A_3^j$ . We may infer this from the following observation. In the coordinate system introduced above (cf. eq. (4.18)), the eigenvector for the third eigenvalue  $\mu_3$  is given by  $v_3 = (0, 0, 1)$ . The eigenvectors  $v_1$  and  $v_2$  both lie in the  $q_1 q_2$ -plane, and since the matrix  $\tilde{\mathcal{M}}$  is degenerate we have the freedom to take them to be orthogonal to the gradient of the corresponding eigenvalue fields. This means that

$$\begin{aligned} v_1 \cdot \nabla \mu_1 &= \mu_{1,1} = 0, \\ v_2 \cdot \nabla \mu_2 &= \mu_{2,2} = 0. \end{aligned} \quad (4.27)$$

This proves the unfolding  $D_4^{ij} \rightarrow A_3^i$  and  $D_4^{ij} \rightarrow A_3^j$ . For the relations between the singularity classes see section 7.1. For a formal proof see [39].

#### *The $D_4$ location*

Shell-crossing for  $A$  caustics is a one-dimensional process. A direct implication of this is that the related critical points are equivalent up to diffeomorphisms. For the  $D$  family this is no longer true. Shell-crossing for the  $D$ -family is two dimensional. As a consequence, the  $D_4$  class consist of hyperbolic ( $D_4^+$ ) and elliptic ( $D_4^-$ ) umbilic points, i.e.

$$D_4^{ij}(t) = D_4^{+ij}(t) \cup D_4^{-ij}(t). \quad (4.28)$$

In order to infer the corresponding caustic conditions we consider the two constraint quantities  $Q_1(q)$  and  $Q_2(q)$  (see eq. (4.25)),

$$\begin{aligned} Q_1(q) &= \frac{M_{11}(q) - M_{22}(q)}{2}, \\ Q_2(q) &= M_{12}(q), \end{aligned} \quad (4.29)$$

which at the  $D_4$  singularity location vanish, i.e.  $Q_1(D_4) = 0$  and  $Q_2(D_4) = 0$ . By a Taylor expansion of  $Q_1(q)$  and  $Q_2(q)$  in a neighbourhood around the  $D_4$  singularity, we find that for points located in the  $q_1 q_2$ -plane,

$$\begin{aligned} Q_1(q) &= a q_1 + b q_2, \\ Q_2(q) &= c q_1 + d q_2. \end{aligned} \quad (4.30)$$

In this expansion, we have taken the  $D_4$  singularity to define the origin of the coordinate system. In this expansion, the parameters  $a, b, c$  and  $d$  are the derivatives of  $Q_1(q)$  and  $Q_2(q)$  at the  $D_4$  location,

$$a = \frac{1}{2} \frac{\partial(M_{11} - M_{22})}{\partial q_1}, \quad b = \frac{1}{2} \frac{\partial(M_{11} - M_{22})}{\partial q_2}, \quad c = \frac{\partial M_{12}}{\partial q_1}, \quad d = \frac{\partial M_{12}}{\partial q_2}. \quad (4.31)$$

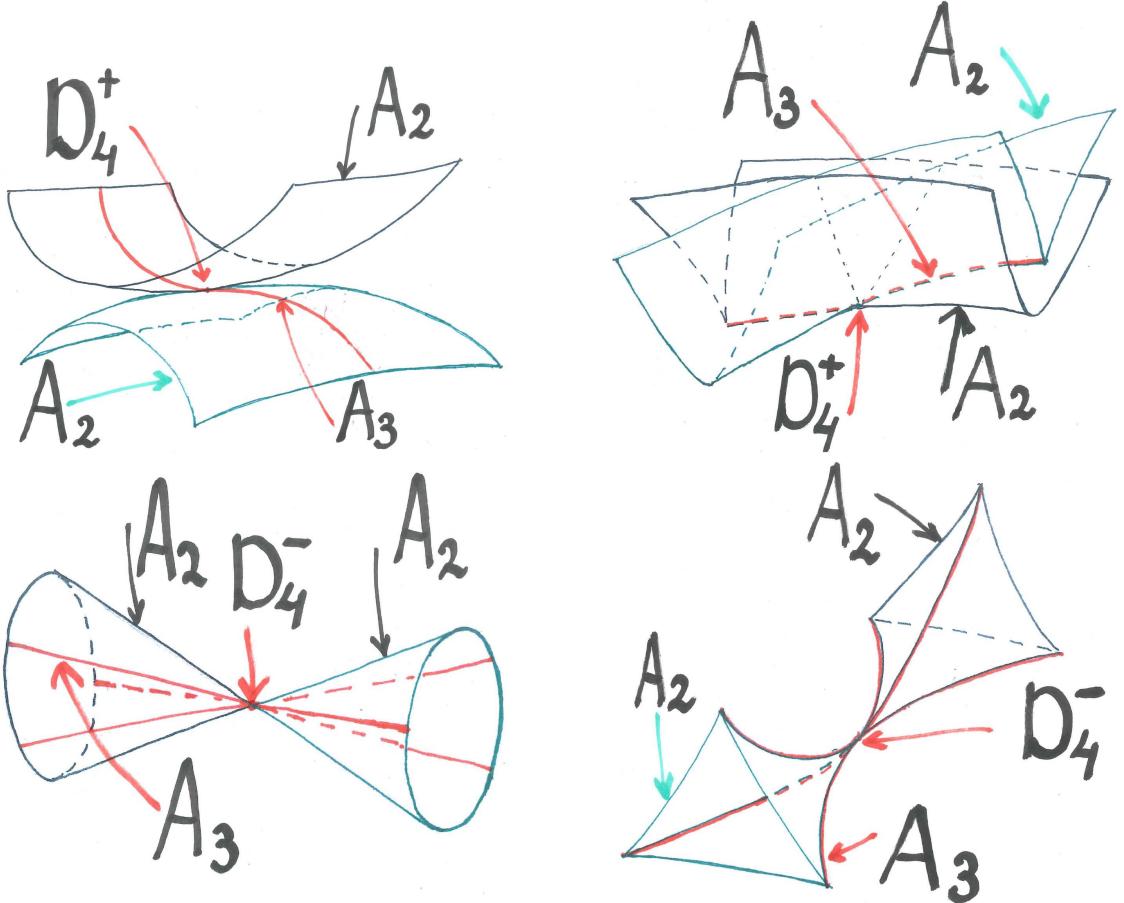


**Figure 13:** The hyperbolic/elliptic umbilic ( $D_4^\pm$ ) singularities. The upper two panels show the elliptic umbilic ( $D_4^+$ ) singularity. The lower panels show the hyperbolic umbilic ( $D_4^-$ ) singularity. The two panels on the left are their representations in Lagrangian space and the two panels on the right their representation in Eulerian space. The black sheets are fold ( $A_2$ ) sheets corresponding to one eigenvalue field. The green sheets are fold ( $A_2$ ) sheets corresponding to a second eigenvalue field. The red lines are cusp ( $A_3$ ) curves. The point in the center depict the hyperbolic/elliptic umbilic ( $D_4^\pm$ ) singularities. The hyperbolic umbilic ( $D_4^+$ ) and elliptic umbilic ( $D_4^-$ ) singularity are also known as the purse and pyramid singularity.

As proposed by [28], the determinant  $S_{\mathcal{M}}$  of the corresponding  $Q_1 Q_2$  map,

$$S_{\mathcal{M}} = bc - ad = \frac{1}{2} [(M_{112} - M_{222})M_{112} - (M_{111} - M_{122})M_{122}] , \quad (4.32)$$

is invariant under rotations in the  $q_1 q_2$ -plane <sup>8</sup>. In the expression above, we have used the notation

$$M_{iik} = \frac{\partial M_{ii}}{\partial q_k}, \quad M_{ikk} = \frac{\partial M_{ik}}{\partial q_k} . \quad (4.33)$$

---

<sup>8</sup>In fact, it can be shown that this determinant is a third-order invariant under rotations [28].

Using the relations between the matrix elements  $M_{11}$ ,  $M_{22}$  and  $M_{12}$  and the eigenvalues  $\mu_1$  and  $\mu_2$ , we may recast the determinant  $S_{\mathcal{M}}$  in an explicit expression incorporating these eigenvalues,

$$S_{\mathcal{M}} = \frac{1}{2} [(\mu_1 - \mu_2)_{,2} \mu_{1,2} - (\mu_1 - \mu_2)_{,1} \mu_{2,1}] . \quad (4.34)$$

As [28] pointed out, the transformation can be shown to consist of two branches. Their identification surfaces via a rescaling of the determinant via the multiplication by a *positive* number. We then find that the two branches correspond to two separate singularity classes of the  $D_4$  family,

$$D_4^{\pm ij}(t) = \{q \in L | q \in A_2^i(t) \cap A_2^j(t) \wedge \text{sign}(S_{\mathcal{M}}) = \pm 1\} , \quad (4.35)$$

where the points  $q \in A_2^i(t) \cap A_2^j(t)$  are the points for whom at time  $t$  the caustic conditions are simultaneously valid for two eigenvalues, i.e.  $1 + \mu_i = 1 + \mu_j = 0$ . Integrated over time, these  $D_4^{\pm ij}(t)$  points trace out the curves  $D_4^{\pm ij}$ ,

$$D_4^{\pm ij} = \{q \in L | q \in A_2^i(t) \cap A_2^j(t) \wedge \text{sign}(S_{\mathcal{M}}) = \pm 1, \text{ for some time } t\} . \quad (4.36)$$

#### 4.2.2 The $D_4^{\pm}$ points

The topology of the  $D_4^{\pm ij}(t)$  variety changes at  $D_4^{\pm}$  and  $D_5$  points.

The  $D_4^{\pm}$  points are analogous to the  $A_4^{\pm}$  points of the  $A$ -family. The  $D_4^{\pm}$  points occur when  $i$ th and  $j$ th eigenvalue field,  $\mu_i$  and  $\mu_j$ , restricted to the points  $q$  in the  $D_4^{\pm ij}$  variety reaches a minimum or maximum, i.e.

$$\begin{aligned} D_4^{ij+} &= \{q \in L | q \in D_4^{+ij}(t) \wedge \mu_{tk}(q) \text{ max-/min. of } \mu_{tk}|_{D_4^{+ij}}(k = i \text{ or } k = j) \text{ for some } t\} \\ D_4^{ij-} &= \{q \in L | q \in D_4^{-ij}(t) \wedge \mu_{tk}(q) \text{ max-/min. of } \mu_{tk}|_{D_4^{-ij}}(k = i \text{ or } k = j) \text{ for some } t\} \end{aligned} \quad (4.37)$$

Particularly interesting is the fact that the  $D_4^{\pm}$  points are always created as a pair. Two  $D_4^+$  points are created simultaneously, as are  $D_4^-$  points. By implication, also the  $D_4^{\pm}$  curves (eq. (4.36)) are always created in pairs. This is in contrast to the  $D_5$  points, which go along with the creation of a pair consisting of a  $D_4^+$  and a  $D_4^-$  point.

#### 4.2.3 The $D_5$ caustics

The shell-crossing condition applied to the  $D_4^{ij}$  variety yields the caustic conditions for the  $D_5$  parabolic umbilic singularity.

The manifold  $D_4^{ij}$  forms a singularity in the point  $q_s \in D_4^{ij}(t)$  if and only if the tangent vector  $T \in T_{q_s} D_4^{ij}$  is normal to  $v_k$ , with  $k \neq i, j$ . Hence, the normal,  $n = \nabla(\mu_{ti} - \mu_{tj})$ , is orthogonal to both  $v_i$  and  $v_j$ ,

$$\begin{aligned} (\mu_i - \mu_j)_{,i} &\equiv v_i \cdot \nabla(\mu_{ti} - \mu_{tj}) = 0 , \\ (\mu_i - \mu_j)_{,j} &\equiv v_j \cdot \nabla(\mu_{ti} - \mu_{tj}) = 0 . \end{aligned} \quad (4.38)$$

The collection of all such points

$$D_5^{ij} = \{q \in L | q \in D_4^{ij}(t) \wedge (\mu_i - \mu_j)_{,i} = (\mu_i - \mu_j)_{,j} = 0 \text{ for some time } t\} . \quad (4.39)$$

The elliptic and hyperbolic umbilic ( $D_4^\pm$ ) points merge in parabolic umbilic ( $D_5$ ) points, since  $D_5^{ij}(t) \subset D_4^{ij}(t)$  and

$$S_{\mathcal{M}} = \frac{1}{2} \{(\mu_i - \mu_j)_{,j} \mu_{i,j} - (\mu_i - \mu_j)_{,i} \mu_{j,i}\} = 0. \quad (4.40)$$

The  $D_5$  points are stable singularities in the classification of Lagrangian singularities. For general dynamics they are unstable and not included in the classification scheme.

## 5 Classification of singularities

The form and morphology in which the various singularities that were inventorized in the previous section will appear in the reality of a physical system depends on several aspects. The principal influence concern the dynamics of the system, as well as its dimensionality. The dynamics determines the way the fluid evolves, to a large extent via its dominant influence on the accompanying flow of the fluid. This affects the morphology of the fluid, and in particular the occurrence of singularities. Evidently, also the dimensionality of the fluid process will bear strongly on the occurrence and appearance of singularities. Higher spatial dimensions may enlarge the number of ways in which a singularity may form. It also influences the ways in which singularities can dynamically transform into one another.

In this section, we provide an impression of the variety in appearance of singularities. To this end, we will first discuss the generic singularity classification scheme that we follow. It is not the intention of this study to provide an extensive listing of all possible classes of fluids. Instead, to make clear in how different physical situations may affect the appearance of singularities, we restrict our presentation of classification schemes to two different classes of fluids. We also restrict our inventory to fluids in a three-dimensional context. It is the most representative situation, and at the same time offers a good illustration of other configurations.

### 5.1 Classes of Lagrangian fluids

To appreciate the role of the dynamics in constraining the evolution and appearance of a fluid, and that of the formation and fate of the singularities in the fluid, it is important to understand and describe its evolution in terms of six-dimensional phase space.

One way of defining phase space  $\mathcal{C}$  is in terms of the Cartesian product of Lagrangian and Eulerian manifolds  $L$  and  $E$ , i.e.  $\mathcal{C} = L \times E$ . In this context, the phase space coordinates of a mass element are  $(q, x)$ . Every point in phase space  $(q, x) \in \mathcal{C}$  represents the initial and final position  $q$  and  $x$  of a mass element at some time  $t$ . Evidently, one may also opt for the more conventional definition consisting of space coordinates  $x$  and canonical momenta  $p$ , in which case the phase space coordinate of a mass element are given by  $(x, p)$ . However, for the description of Lagrangian fluid dynamics it is more convenient to follow the first convention. We should note that for this description of phase space Liouville's theorem does not apply, specifically not for the Euclidean notion of volumes.

At the initial time  $t = 0$ , the Lagrangian map is the identity map, i.e. for all  $q \in L$   $x_0(q) = q$ . In phase space  $\mathcal{C}$ , the fluid then occupies the submanifold  $\mathcal{L}_0 = \{(q, x_0(q)) \in \mathcal{C} | q \in L\}$ . If we equip  $\mathcal{C}$  with a symplectic structure  $\omega$ , we can prove this to be a so-called Lagrangian submanifold (for a precise definition of Lagrangian submanifolds see appendix B).

Differences in the dynamics of a fluid reveal themselves in particular through major differences in the phase space structure and topology of the manifolds delineated by the mass

elements. To provide an impression of the differences in morphology and classification of singularities emerging in fluids of a different nature, specifically that of fluids with a different dynamical behaviour, we concentrate the discussion on two different classes of Lagrangian fluids:

1. *Generic Lagrangian fluids.*

Lagrangian fluids for which the map  $x_t : L \rightarrow E$  is a generic continuous and differentiable mapping from  $L$  to  $E$  for every time  $t$ . The dynamics does not restrict the map  $x$  to any extent. We describe the classification up to local diffeomorphisms, i.e. two singularities are considered equivalent if and only if there exist local coordinate transformations, which map them into each other.

2. *Lagrangian fluids with Hamiltonian dynamics.*

The evolution of the fluid is governed by a Hamiltonian. This assumption restricts the possible evolution of the fluid. Formally, the map  $x$  corresponds uniquely to a so-called Lagrangian map. The singularities of Lagrangian maps, known as Lagrangian singularities, are classified up to Lagrange equivalence.

Lagrangian fluids with Hamiltonian dynamics form an important class of fluids: fundamental theories of particle physics generally allow for a Hamiltonian description. Nonetheless, in a range of practical circumstances we may encounter fluids that are either more or less constrained. An example are fluids with effective dynamics. They contain friction terms which are not described by Hamiltonian systems. Such fluid systems are less restrictive than those that are specifically Hamiltonian. On the other hand, there are also Hamiltonian fluids that are characterized by additional constraints.

Systems that are characterized by either more or less constraints may involve different classification schemes than regular Hamiltonian fluids. While it is beyond the scope of this study to provide a complete, and exhaustive, inventory of all classification scheme, the comparison between the classification schemes of two different fluid configurations will provide an impression of the variety. The principal intention is to provide an understanding of the robustness of Hamiltonian systems.

## 5.2 Singularity classification

As we observed at the beginning of this paper (see eqn. (2.6)), singularities form when  $\mu_i + 1 = 0$  for at least one  $i$ . The emerging singularities can be classified into several families. Here we follow the classification scheme defined by Bruce [16] for singularities of generic one-family maps  $x(q) : L \rightarrow E$ .

For practical reasons, we restrict the presentation of the classification to the case of  $L$  and  $E$  being three-dimensional spaces. We also restrict ourselves to the classification of stable singularities. Stability in this sense means that the singularities do not change in character when a small fluctuation is applied to the Lagrangian map. It means that if the map  $x_t$  has a stable singularity in point  $p$  at time  $t$ , then the map  $x_t + \delta x_t$  with  $\delta x_t$  sufficiently small, has a singularity in the same equivalence class at a point close to  $p$  at a time close to  $t$ . Because in practical situations unstable singularities only have a probability measure zero to occur, we will not include them in our consideration.

For the situation of three-dimensional fluids, we may use the formal criterion of their corank to split the equivalence classes of singularities into three groups. The corank of a matrix is defined as the number of spatial dimensions minus the rank of the matrix. It leads to the following scheme, in which we recognize the singularities identified in the previous sections,

---

*A<sub>k</sub> class.*

When the deformation tensor  $\mathcal{M}$  is non-invertible due to one eigenvalue, it has corank 1. These singularities are classified by the  $A_k$  classes.

*D<sub>k</sub> class.*

When  $\mathcal{M}$  is non-invertible due to two eigenvalues, the singularity has co-rank 2. Singularities with co-rank 2 are classified as  $D_k$  classes.

*E<sub>k</sub> class.*

In 3-dimensional fluids, the points for which the Hessian has co-rank 3 is of measure zero. Following this observation, we do not consider these  $E_k$  class singularities.

---

Given that the  $E_k$  singularities in practice will never occur, we will restrict the discussion of the singularity classification scheme to the  $A_k$  and  $D_k$  classes.

### 5.3 Singularity classification: generic fluids

For the classification of singularities of generic one-family maps  $x : L \rightarrow E$ , with  $L$  and  $E$  three-dimensional, we follow the classification by [16]. Important for our purpose, is that it can be shown that the singularities that may emerge in generic mappings from  $L \rightarrow E$  are equivalent to those emerging in the simple linear maps

$$x_t(q) = q + t u(q), \quad (5.1)$$

in which  $u$  is a vector field on  $L$ . In general, the vector field  $u(q)$  contains both a longitudinal and a transversal part,

$$u(q) = u_l(q) + u_t(q). \quad (5.2)$$

The longitudinal component corresponds to potential motion and has curl zero,  $\nabla \times u_l = 0$ , while the transversal component has divergence zero,  $\nabla \cdot u_t = 0$ . When the motion is restricted to its longitudinal component, the displacement  $s_t(q)$  effectively is that of ballistic motion.

The classification of singularities in general Lagrangian fluid dynamics is expressed by theorem 3. We restrict ourselves to listing the classification scheme of Bruce [16], in terms of the generic expressions for the maps  $x_t(q)$  of each of the classified singularities. The maps  $x_t(q)$  in the corresponding table assume that the singularity occurs at the origin  $q = 0$ , at  $t = 1$ . In appendix C we show that these normal forms indeed satisfy the corresponding caustic conditions. For the proofs and in-depth derivations we refer to Bruce [16].

**Theorem: 3** *A stable singularity occurring in a Lagrangian fluid with generic dynamics is, up to local diffeomorphisms, equivalent to one of the following classes:*

<i>Singularity class</i>	<i>Map</i> $x_t(q)$	<i>Singularity name</i>
$A_1$	$x_t(q) = q$	<i>trivial case</i>
$A_2$	$x_t(q) = q + t(0, 0, q_3^2 - q_3)$	<i>fold</i>
$A_3$	$x_t(q) = q + t(0, 0, q_1 q_3 + q_3^3 - q_3)$	<i>cusp</i>
$A_4$	$x_t(q) = q + t(0, 0, q_1 q_3 + q_3^4 - q_3)$	<i>swallowtail</i>
$A_5$	$x_t(q) = q + t(0, 0, q_1 q_3 + q_2 q_3^2 + q_3^5 - q_3)$	<i>butterfly</i>
$D_4^\pm$	$x_t(q) = q + t(0, q_2 q_3 - q_2, q_2^2 \pm q_3^2 + q_1 q_2 - q_3)$	<i>hyperbolic/elliptic</i>
$A_3^\pm$	$x_t(q) = q + t(0, 0, (q_1^2 \pm q_2^2)q_3 + q_3^3 - q_3)$	
$A_4^\pm$	$x_t(q) = q + t(0, 0, q_1 q_3 \pm q_2^2 q_3^2 + q_3^4 - q_3)$	

*Note:* The expressions in the table assume that the singularity occurs at the origin  $q = 0$ , at  $t = 1$ . The first five singularity classes are the  $A$ -family. The subsequent class is the  $D$ -family. The last two are the normal forms of the  $A_3$  and  $A_4$  points. The  $A_k$  class has co-rank 1 and co-dimension  $k - 2$ . The  $D_4^\pm$  singularities have co-rank 2 and are one-dimensional [16].

#### 5.4 Singularity classification: Hamiltonian fluids

The evolution of Lagrangian fluids with Hamiltonian dynamics is more constrained than that of generic Lagrangian fluids. As the fluid develops complex multistream regions, the phase space submanifold  $\mathcal{L}_t = \{(q, x_t(q)) | q \in L\}$  for fluids with Hamiltonian dynamics remains Lagrangian. For generic fluid dynamics this is no longer true.

A key step in evaluating the emerging singularities is that of connecting the displacement map  $s_t(q)$  to the Lagrangian map. In appendix B.2, we describe in some detail how a given Lagrangian map can be constructed from a Lagrangian submanifold  $\mathcal{L}$ . A Lagrangian map can develop regions in which multiple points in the Lagrangian manifold are mapped to the same point in the base space.

Lagrangian singularities are those points at which the number of pre-images of the Lagrangian map undergoes a change. Lagrangian catastrophe theory [5, 12] classifies the stable singularities. This refers to the stability of singularities with respect to small deformations of the Lagrangian manifold of  $\mathcal{L}$ . This is true up to Lagrangian equivalence, a concept that is a generalization of equivalence up to coordinate transformation. For a more formal and precise definition of Lagrangian equivalence see appendix B.

It can be demonstrated [see 12] that every Lagrangian map  $l : \mathcal{L} \rightarrow \mathcal{C} \rightarrow E$  is locally Lagrangian equivalent to a so-called gradient map. In other words, it means the corresponding map  $x_t$  is locally equivalent to

$$x_t(q) = \nabla_q S_t, \quad (5.3)$$

in which  $S_t : L \rightarrow \mathbb{R}$ , for all  $q$  and  $t$ , is a scalar function. By recasting  $S_t$  in terms of a function  $\Psi_t : L \rightarrow \mathbb{R}$ ,

$$S_t = \frac{1}{2}q^2 + \Psi_t(q), \quad (5.4)$$

we find that locally the map  $x$  can be written in the form

$$x_t(q) = q + \nabla_q \Psi_t(q). \quad (5.5)$$

Evidently, this implies that the displacement map is longitudinal, and that the corresponding Jacobian  $\partial s_t / \partial q$  is symmetric.

The classification of singularities of a Lagrangian fluid with Hamiltonian dynamics is expressed by theorem 4. The classification scheme listed is that of Bruce [16]. Also here, the maps  $x_t(q)$  in the table are for the singularity located at the origin  $q = 0$ , at  $t = 1$ . In appendix C it is shown that these normal forms indeed satisfy the corresponding caustic conditions. For proofs we refer to Bruce [16].

**Theorem: 4** *A stable Lagrangian singularity of a Lagrangian fluid with Hamiltonian dynamics, is locally Lagrange equivalent to one of the following classes:*

Singularity class	Map $x_t(q)$	Singularity name
$A_1$	$x_t(q) = q$	trivial case
$A_2$	$x_t(q) = q + t(0, 0, q_3^2 - q_3)$	fold
$A_3$	$x_t(q) = q + t\left(\frac{1}{2}q_3^2, 0, q_3(q_1 - 1)\right)$	cusp
$A_4$	$x_t(q) = q + t\left(\frac{1}{2}q_3^2, 0, q_1q_3 + q_3^4 - q_3\right)$	swallowtail
$A_5$	$x_t(q) = q + t\left(\frac{1}{2}q_3^2, \frac{1}{3}q_3^3, q_1q_3 + q_2q_3^2 + q_3^5 - q_3\right)$	butterfly
$D_4^\pm$	$x_t(q) = q + t\left(\pm q_1q_2 - q_1, \pm\left(\frac{1}{2}q_1^2 + \frac{3}{2}q_2^2\right) + 2q_2q_3 + 2q_2^3 - q_2, q_2^2\right)$	hyperbolic/elliptic
$D_5$	$x_t(q) = q + t(0, q_2^3 - q_2, q_3^3 - q_3)$	parabolic
$A_3^\pm$	$x_t(q) = q + t\left(q_1q_3^2, \pm q_2q_3^2, (q_1^2 \pm q_2^2)q_3 + q_3^3 - q_3\right)$	
$A_4^\pm$	$x_t(q) = q + t\left(\frac{1}{2}q_3^2, \pm\frac{2}{3}q_2q_3^3, q_1q_3 \pm q_2^2q_3^2 + q_3^4 - q_3\right)$	

*Note: The expressions in the table assume that the singularity occurs at the origin  $q = 0$ , at  $t = 1$ . The first five singularity classes are the  $A$ -family. The subsequent two are the  $D$ -family. The last two are the normal forms of the  $A_3$  and  $A_4$  points. The  $A_k$  class has co-rank 1 and co-dimension  $k - 2$ . The  $D_k$  singularities have co-rank 2 and co-dimension  $k - 2$  [5].*

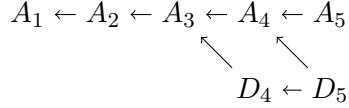
Comparing the classification schemes for generic Lagrangian singularities and those for Lagrangian fluids with Hamiltonian dynamics, we may note the similarities in the classification. Both classifications have an  $A$  and a  $D$  family. It can be demonstrated that the  $A$  singularity classes of the scheme for Lagrangian fluids with Hamiltonian dynamics are contained in those corresponding to the generic Lagrangian fluid. Concretely, this means that a displacement field corresponding to the Hamiltonian  $A_k$  class is also an element of the generic  $A_k$  class. On the other hand, there are significant differences in the case of the  $D$  families.

The  $D$  families are somewhat different. The Hamiltonian  $D_4$  class is contained in the generic  $D_4$  class. However, the Hamiltonian  $D_5$  class has no analogue in the generic classification scheme. This is a result of the  $D_5$  singularity not being stable under coordinate transformations.

A final remark concerns the singularity classification schemes for higher dimensional fluids. For these a more elaborate classification scheme applies. This classification scheme is described in appendix B.

## 5.5 Unfoldings

Singularities generally change their class upon small, but finite, deformations of the displacement map  $s_t$ . The corresponding evolution of a singularity follows the universal unfolding process of singularities. The general behavior is described in the following unfolding diagram, in which the arrows indicate the singularity into which specific singularities can transform.



For  $i \geq 2$ , the  $A_i$  singularities decay into  $A_{i-1}$  singularities. For  $i \geq 5$ , the  $D_i$  singularities decay into either  $A_{i-1}$  or  $D_{i-1}$  singularities. In section 7 we will describe how the decay of singularities is connected to the evolution of the large-scale structure in the Universe and in outlining the spine of the cosmic web.

## 5.6 Density profile

Vesilev [68] inferred the density profiles of the various classes of singularities, in case they emerge as a result of potential motion in a collision-less self-gravitating medium. For each of the mass concentrations in and around these singularities, he found scale free power-law profiles. The radially average profiles display the following decrease of density  $\rho(r)$  as a function of radius  $r$ .

Singularity class	Singularity name	Profile $\rho(r)$
$A_2$	fold	$\rho(r) \propto r^{-1/2}$
$A_3$	cusp	$\rho(r) \propto r^{-2/3}$
$A_4$	swallowtail	$\rho(r) \propto r^{-3/4}$
$A_5$	butterfly	$\rho(r) \propto r^{-4/5}$
$D_4$	hyperbolic/elliptic	$\rho(r) \propto r^{-1}$
$D_5$	parabolic	$\rho(r) \propto r^{-1} \log(1/r)$

With respect to these radially averaged profiles, we should realize that the mass distribution in and around the singularities is highly anisotropic. This is true for any dimension in which we consider the structure around the singularities.

Notwithstanding this, we do observe that the steepest density profiles are those around the point singularities  $A_5$  and  $D_5$ . However, they are mere transient features that will only exist for a single moment in time. The point singularities  $A_4$  and  $D_4$  display a less pronounced behaviour. However, they move over time. Also, we see that the cusp singularity  $A_3$  possesses a steeper mass distribution than that in and around the sheet singularity  $A_2$ .

## 6 The caustic skeleton & the cosmic web

The process of formation and evolution of structure in the Universe is driven by the gravitational growth of tiny primordial density and velocity perturbations. When it reaches a stage at which the matter distribution starts to develop nonlinearities, we see the emergence

of complex structural patterns. In the current universe we see this happening at Megaparsec scales. On these scales, cosmic structure displays a marked intricate weblike pattern, the Cosmic Web. Prominent elongated filamentary features define a pervasive network. Forming the dense boundaries around large tenuous sheetlike membranes, the filaments connect up at massive, compact clusters located at the nodes of the network and surround vast, underdense and near-empty voids.

The gravitational structure formation process is marked by vast migration streams, known as cosmic flows. Inhomogeneities in the gravitational force field lead to the displacement of mass out of the lower density areas towards higher density regions. Complex structures arise at the locations where different mass streams meet up. Gravitational collapse sets in as this happens. In terms of six-dimensional phase space, it corresponds to the local folding of the phase space sheet along which matter – in particular the gravitationally dominant dark matter component – has distributed itself.

The positions where streams of the dark matter fluid cross are the sites where gravitational collapse occurs. The various types of caustics described and classified in our study mark the different configurations in which this process may take place. Their locations trace out a Lagrangian skeleton of the emerging cosmic web, marking key structural elements and establishing their connectivity (also see the discussion in [39]). In other words, the  $A_3, A_4, A_5, D_4, D_5$  varieties, in combination with the corresponding  $A_3^\pm, A_4^\pm$ , and  $D_4^\pm$  points, are the dynamical elements whose connectivity defines the weaving of the the cosmic web [4, 14, 22, 67, 73].

On the basis of this observation, we may obtain the skeleton of the cosmic web in Eulerian space by means of the Lagrangian map  $x_t$  to Eulerian space. Following the identification of the various caustic varieties and caustic points in Lagrangian space, the application of the map  $x_t$  will produce the corresponding weblike structure in Eulerian space.

Of central significance in our analysis and description of the cosmic web is the essential role of the deformation tensor *eigenvector* fields in outlining the caustic skeleton and in establishing the spatial connections between the various structural features. So far, Lagrangian studies of the cosmic web have usually been based on the role of the *eigenvalues* of the deformation tensor (for recent work see [23, 50, 71]). Nearly without exception, they ignore the information content of the eigenvectors of the deformation tensor. In this work we actually emphasize that the eigenvectors are of key importance in tracing the spatial locations of the different types of emerging caustic features and, in particular, in establishing their mutual spatial connectivity. This important fact finds its expression in terms of the *caustic conditions* that we have derived in this study.

The study by Hidding et al. [39] illustrated the important role of the deformation field eigenvectors in outlining the skeleton of the cosmic web, for the specific situation of  $A_3$  cusp lines in the 2-D matter distribution evolving out of a Gaussian initial density field. The present study describes the full generalization for the evolving matter distribution (a) for each class of emerging caustics in (b) in spaces of arbitrary dimension  $D$ .

A telling and informative illustration of the intimate relationship between the caustic skeleton defined by the derived caustic conditions and the evolving matter distribution is that offered by the typical patterns emerging in the two-dimensional situation. Figure 14 provides a direct and quantitative comparison between the caustic skeleton of the cosmic web and the fully nonlinear mass distribution in an N-body simulation. The three panels

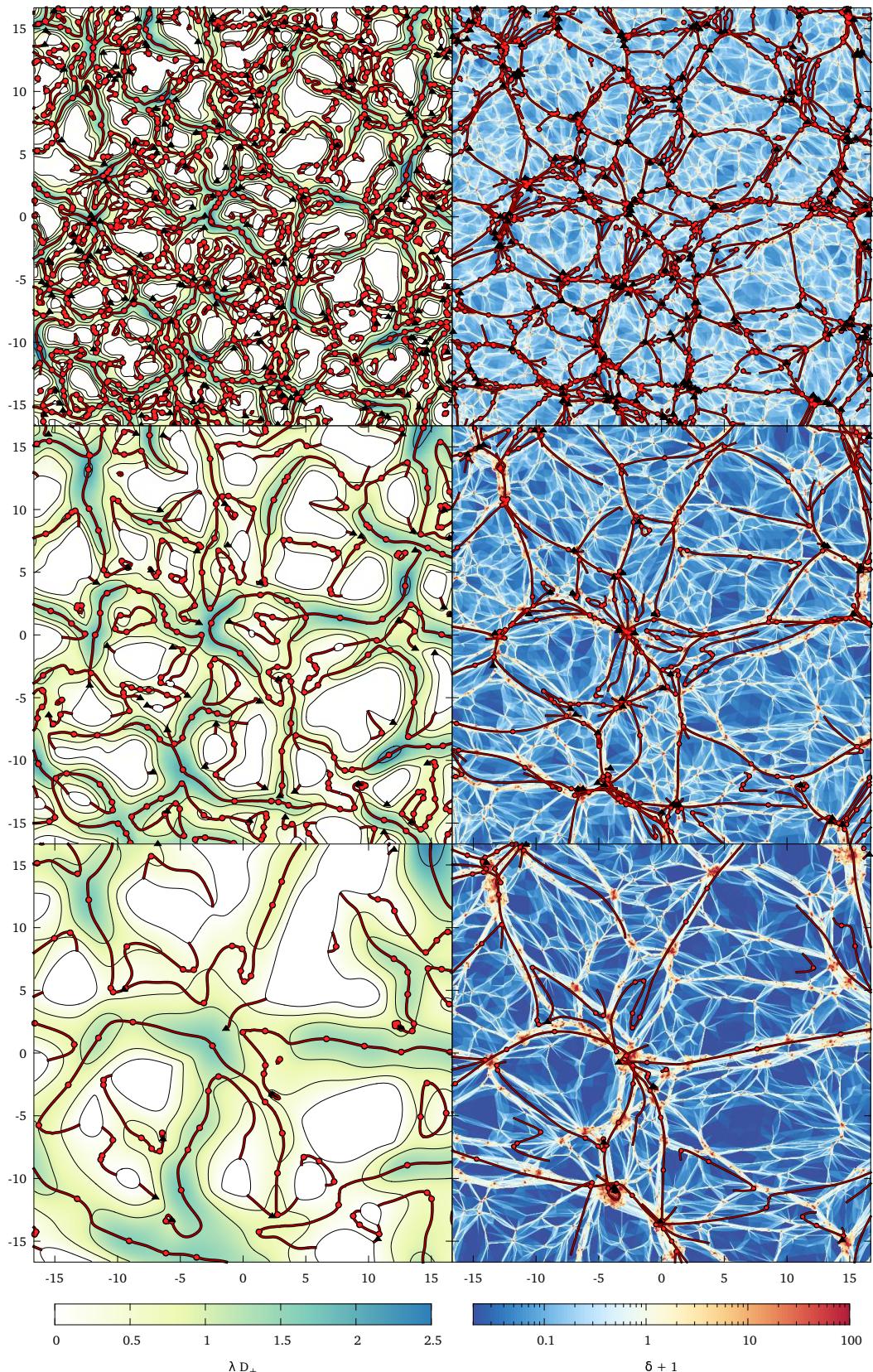


**Figure 14:** Spatial distribution of singularities in the Lagrangian and Eulerian Cosmic Web. The figure compares the spine of the cosmic web with the mass distribution in a 2-D  $N$ -body simulation. Left panel: initial field of density fluctuations and the skeleton of identified singularities/catastrophes. Right panel: density field of an evolved 2D cosmological  $N$ -body simulation, in which the Lagrangian skeleton of singularities is mapped by means of the Zel'dovich approximation. From Feldbrugge et al. [33].

in the lefthand column show the Lagrangian skeleton for a two-dimensional fluid. The fluid is taken to evolve according to the Zel'dovich approximation [73] (see appendix A), which represents a surprisingly accurate first-order Lagrangian approximation of a gravitationally evolving matter distribution [see e.g. 64]. The initial density field of the displayed models is that of a Gaussian random density field [2, 13], which according to the latest observations and to current theoretical understanding is an accurate description of the observed primordial matter distribution [27, 46, 56].

To enable our understanding of the hierarchical process of structure formation and the resulting multiscale structure of the cosmic web, we assess the caustic structure of the Lagrangian matter field at three different resolutions. In figure 14 the field resolution decreases from the top panels to the bottom panels, as the initial density field was smoothed by an increasingly large Gaussian filter. The contour maps that form the background in these panels represent the resulting initial density fields. The red lines trace the  $A_3$  variety, i.e. the  $A_3$  lines, for the largest eigenvalue  $\mu_1$  field (also see fig. 4 to appreciate how they are related). Also the  $A_3^\pm$  points and  $D_4^\pm$  points are shown, the first as red dots, the latter as black triangles.

The resulting weblike structure in Eulerian space is depicted in the corresponding right-hand panels. The  $A_3$  lines,  $A_3^\pm$  points and  $D_4^\pm$  points are mapped to their Eulerian location by means of the Zel'dovich approximation. The red lines, red dots and black triangles represent the Eulerian skeleton corresponding to the Zel'dovich approximation. These are superimposed on the density field of the corresponding N-body simulations. The comparison between the latter and the Eulerian skeleton reveal that the caustic skeleton – the assembly of  $A_3$  lines,  $A_3^\pm$  points and  $D_4^\pm$  points – trace the principal elements and connections of the cosmic web seen in the N-body simulations remarkably well (see table 1 for the identification of the lines and points to the cosmic web). Moreover, by assessing the caustic structure at different resolutions of the density field, one obtains considerable insight into the multiscale structure and topology of the cosmic web.

One of the unique features facilitated by the caustic conditions that we have derived in the previous sections is the ability to go beyond the two-dimensional case and construct and explore the full caustic skeleton of the three-dimensional mass distribution. In the case of the skeleton of the cosmic web defined by the three-dimensional mass distribution, the cusp ( $A_3$ ) sheets correspond to the walls or membranes of the large scale structure [14, 22, 52, 67]. The swallowtail ( $A_4$ ) and elliptic/hyperbolic umbilic ( $D_4^\pm$ ) lines correspond to the filaments of the cosmic web and the butterfly ( $A_5$ ) and parabolic umbilic ( $D_5$ ) points correspond to the cluster nodes of the network [3, 14, 22, 52, 67]. The identification of the caustics in the three dimensional cosmic web is summarized in table 1.

To appreciate the impressive level at which the caustic skeleton is outlining the three-dimensional weblike mass distribution, figure 15 provides an instructive illustration. The figure depicts elements of the caustic skeleton of the Zel'dovich approximation in a  $200h^{-1}$

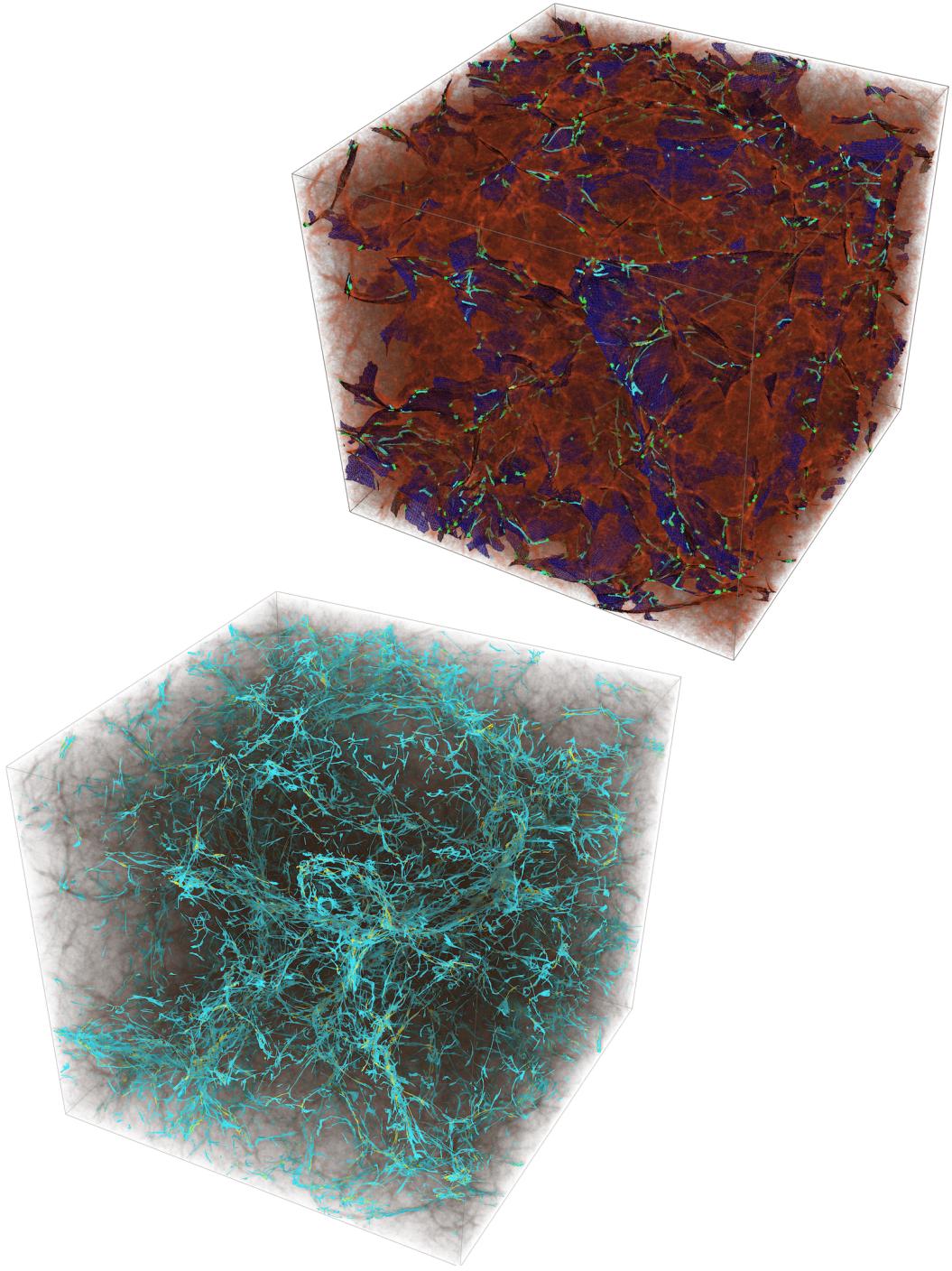


**Figure 15:** The log density field of a dark matter  $N$ -body simulation with  $\Lambda$ CDM cosmology in a box of  $200h^{-1}$  Mpc with  $512^3$  particles and elements of the caustic skeleton of the Zel'dovich approximation [52]. Top right panel: the cusp ( $A_3$ ) sheets (dark blue), the swallowtail ( $A_4$ ) lines (light blue) and the elliptic/hyperbolic umbilic lines (yellow) corresponding to the lowest eigenvalue field of the caustic skeleton. The initial density field was smoothed on the scale  $6.3h^{-1}$  Mpc. Bottom left panel: the swallowtail ( $A_4$ ) lines (light blue) and the elliptic/hyperbolic umbilic lines (yellow) corresponding to the lowest eigenvalue field of the caustic skeleton. The initial density field is smoothed at  $3.1h^{-1}$  Mpc.

Singularity class	Singularity name	Feature in the 2D cosmic web	Feature in the 3D cosmic web
$A_2$	fold	collapsed region	collapsed region
$A_3$	cusp	filament	wall or membrane
$A_4$	swallowtail	cluster or knot	filament
$A_5$	butterfly	not stable	cluster or knot
$D_4$	hyperbolic/elliptic	cluster or knot	filament
$D_5$	parabolic	not stable	cluster or knot

**Table 1:** The identification of the different caustics in the 2- and 3-dimensional cosmic web

Mpc box. The resulting skeleton is superposed on the log density field of a dark matter  $N$ -body simulation in a  $\Lambda$ CDM cosmology with  $512^3$  particles [52]. We should emphasize that the Zel'dovich approximation is linear and that the corresponding skeleton is completely local in the initial conditions. While a full and detailed analysis of these three-dimensional weblike patterns is the subject of an upcoming accompanying paper [32], the illustrations of figure 15 already give a nice impression of the ability of the caustic conditions to outline the spine of the cosmic web.

The top righthand panel contains the cusp ( $A_3$ ) sheet (dark blue colour) and the swallowtail ( $A_4$ ) and elliptic/hyperbolic umbilic ( $D_4^\pm$ ) lines (light blue colour) corresponding to the lowest eigenvalue field, superimposed on the density field of the  $N$ -body simulation (red shaded log density field values). The pattern concerns the caustics obtained for a displacement field that is filtered at a length scale of  $6.3h^{-1}$  Mpc. Close inspection reveals the impressive correspondence between the cusp sheets of the caustic skeleton and the flattened - two-dimensional - features in the mass distribution of the cosmic web. Notwithstanding this, one may also observe that the two-dimensional skeleton does not capture all the structures present in the  $N$ -body simulation. This is predominantly an issue of scale, as the corresponding displacement field cannot resolve and trace features whose size is more refined than the  $6.3h^{-1}$  Mpc filter scale.

An impression of the more refined structure can be obtained from the bottom left panel of figure 15, which follows the line-like elements of the caustic skeleton at a length scale of  $3.1h^{-1}$  Mpc. More specifically, it shows the swallowtail ( $A_4$ ) and elliptic/hyperbolic umbilic ( $D_4^\pm$ ) lines of the caustic skeleton. The correspondence of these with the prominent and intricate filamentary pattern in the cosmic mass distribution is even more outstanding than that of the  $A_3$  sheets with the membranes in the density field. It is important to realize, and emphasize, that apparently we do not need to involve the second eigenvalue to create a filament in the network of caustics. In other words, collapse along the second eigenvector is not necessary to create a filament-like structure (also see [39]). This leads to a radical new insight on structure formation, in that it suggests the existence of different possible late-time morphologies for filaments [40]. We may even relate this to the prominence of the corresponding filamentary features: as they concern features that have experienced collapse along two directions, the umbilic  $D_4^\pm$  filaments will have a higher density and contrast than the filigree of more tenuous  $A_4^\pm$  filaments. An additional observation of considerable interest is that the line-like  $A_4$  and  $D_4^\pm$  features trace the connectivity of the cosmic web in meticulous detail.

## 6.1 Higher order Lagrangian perturbations

Evidently, the details of the dynamical evolution will bear a considerable influence on the developing caustic structure. This not only concerns the dynamics of the system itself, but also its description. The examples that we presented in the previous sections showed the caustic features developing as the dynamics is predicated on the first-order Lagrangian approximation of the Zel'dovich formalism [73]. The visual comparison with the outcome of the corresponding  $N$ -body simulations demonstrated the substantial level of agreement. Nonetheless, given the nature of singularities, the process of caustic formation might be very sensitive to minor deviations of the mass element deformations and hence the modelling of the dynamics. This may even strongly affect the predicted population of caustics and their spatial organization in the skeleton of the cosmic web. Some indications on the level to which the spatial mass distribution is influenced may be obtained from an early series of papers by Buchert and collaborators [17–21], who were the first to explore the formation of structure in higher-order Lagrangian perturbation schemes and investigate in how far they would effect the occurrence and location of multistream regions. An important finding from their work is that 2nd order effects are substantial, while 3rd order ones are minimal. Elaborated and augmented by additional work [15, 61], 2nd order Lagrangian perturbations – usually designated by the name 2LPT – have been established as key ingredients of any accurate analytical modeling of cosmic structure growth. In a follow-up to the present study, we investigate in detail the repercussions of different analytical prescriptions for the dynamical evolution of the cosmic mass distribution for the full caustic skeleton of the cosmic web.

In addition to 2LPT, we will systematically investigate the caustic skeleton in the context of the *adhesion approximation* [35, 36, 38, 41, 64, 69]. Representing a fully nonlinear extension of the Zel'dovich formalism, it includes an analytically tractable gravitational source term for the later nonlinear stages. It accomplishes this via an artificial viscosity term that emulates the effects of gravity, resulting in the analytically solvable Burger's equation. With the effective addition of a gravitational interaction term for the emerging structures, unlike the Zel'dovich approximation the adhesion model is capable of following the hierarchical buildup of structure and the cosmic web [38, 40, 41]. At early epochs, the resulting matter streams coincide with the ballistic motion of the Zel'dovich approximation. At the later stages, as the mass flows approach multistream regions a solid structure is created at the shell-crossing location. Matter inside these structures is confined to stay inside, while outside collapsed structures the results from the Zel'dovich approximation and adhesion are identical. The caustics from the Zel'dovich approximation are compressed to infinitesimally thin structures, hence unifying the Zel'dovich' idea of collapsed structures in terms of shell crossing with a hierarchical formation model. While offering a complete model for the formation and hierarchical evolution of the cosmic web, it does accomplish this by seriously altering the flow pattern involved in the buildup of cosmic structure. This, in turn, is expected to affect at least to some extent the properties and evolution of the caustic population and its connectivity.

## 6.2 Gaussian statistics of the caustic skeleton

In addition to characterizing the geometric and topological outline of the cosmic web in terms of the caustic skeleton, our study points to another important and related application of the formalism described. The fact that the linear Zel'dovich approximation provides such an accurate outline of the skeleton of the cosmic web establishes an important relation between the primordial density and flow field and the resulting cosmic web. Via the Zel'dovich approximation, we may relate the caustic skeleton directly to the statistical nature and characteristics

of the primordial density field. In other words, we may directly relate the structure of the cosmic web to the nature of the Gaussian initial density field. This, in turn, establishes a direct link between the geometric and topological properties of the cosmic web and the underlying cosmology. In other words, our analysis of the caustic skeleton may define a path towards a solidly defined foundation and procedure for using the structure of the observed cosmic web towards constraining global cosmological parameters and the cosmic structure formation process.

The fact that we may invoke Gaussian statistics facilitates the calculation of a wide range of geometric and topological characteristics of the cosmic web, as they are directly related to the primordial Gaussian deformation field, its eigenvalues and eigenvectors. For an example of such a statistical treatment of 2-dimensional fluids, we refer to [31]. It describes how one may not only analytically compute the distribution of maxima, or minima, but also the population of singularities and the length of caustic lines. In an accompanying study, we present an extensive numerical analysis of the statistics of 2- and 3-dimensional caustic skeleton will follow in [32]. This will establish the reference point for the subsequent solid analytical study of interesting geometric properties of the cosmic web (for the initial steps towards this program see [33]).

This will represent a major extension of statistical descriptions that were solely based on the eigenvalue fields. The latter would make it possible to study the number density of clusters and void basins, make predictions on the statistical properties of angular momentum, and even several aspects of the cosmic skeleton (e.g. [29, 57]). In this context it is also relevant to realize that the meaning of eigenvalues extends beyond that known for potential deformation fields, as in more general situations they may have a complex value related to the presence of vorticity in the matter flow field. Nonetheless, as we have argued extensively in previous sections, it is only by invoking the information contained in the corresponding eigenvector fields that we may expect to obtain a more complete census of intricate spatial properties of the cosmic web.

## 7 Dynamics and evolution of caustics

The caustic conditions presented in this study reveal the profound relationship between the various classes of singularities that may surface in fluids. Besides the aspect of the identification and classification of singularities, we need to have insight in the transformation and evolution of caustics and caustic networks that accompanies the dynamical evolution of a fluid. The evolution of the fluid, dictated by the dynamics of the system, generally involves the development of ever more distinctive structures and the proliferation of complex structural patterns.

Tracing the evolution of a fluid starts at an initial time  $t = 0$ . At that time, the displacement map  $s_t$  is the zero map. Amongst others, this implies the fluid does not (yet) contain singularities. Starting from these near uniform initial conditions, the structure in the evolving fluid becomes increasingly pronounced. The phase space sheet that it occupies in six-dimensional space gets increasingly folded. Its projection on Euclidian space follows this process, and it is as a result of the folding process that we see the fluid developing singularities. While the dynamical evolution proceeds to ever more advanced stages, we not only see the appearance of more singularities, but also the transformation of one class of singularities into another one. A complementary process that may underlie the changes of local geometry that

of the merging of singularities into a new singularity, itself a manifestation of the hierarchical buildup of structural complexity.

The eigenvalue landscape in figure 4 offers an instructive tool for facilitating and guiding our understanding and visual intuition for the iterative folding of singularities in phase space and the accompanying caustic transformations.

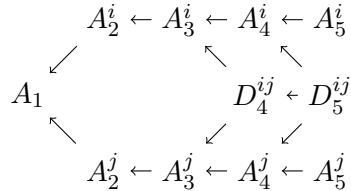
### 7.1 Caustic mutations and transformations: evolutionary sequence

The dynamical evolution of a fluid goes along with a rich palette of local processes. These involve fundamental mutations in the local singularity structure that lead to significant topological changes of the spatial pattern forming in the fluid. In some systems and situations this will be a key element in the hierarchical buildup of structure. Another example where we can recognize such transformations is in the cascade of turbulent features down to ever smaller scales in the still largely understood process of turbulence.

The fundamental notion in these structural mutations in the evolving fluid is that of the ruling dynamics of the system evoking changes in the deformation field. Small deformations will lead to the decay of singularities into different ones belonging to other singularity classes. Conversely, they may get folded according to a rigid order.

The sequence of singularity mutations is not random and arbitrary. Due to the strict geometric conditions and constraints corresponding to the various singularities, expressed in the caustic conditions discussed extensively in this study, a given singularity is only allowed to transform into a restricted set of other singularities. Conversely, a given singularity may only have emanated from a restricted set of other singularities.

In most situations a particular singularity can have decayed from only one distinctive class of singularities. Some may have descended from two other singularity classes. Likewise, most singularities can decay only into one distinctive other class of singularity. This is true for all  $A$ -family singularities.  $D$ -family singularities have a richer diversity of options, with the  $D_5$  points being able to decay into 3 different ones, while the  $D_4$  points may decay into 2 distinct  $A_3$  points. The entire singularity transformation and unfolding sequence may be transparently summarized in the unfolding diagram below.



The unfolding diagram follows directly from Lagrangian catastrophe theory, although it can also be derived from the caustic conditions. The unfoldings of an  $A_k^i$  singularities into an  $A_{k-1}^i$  singularities, with  $k \geq 2$ , follow trivially from the caustic conditions. The same holds for the unfolding of the  $D_5^{ij}$  singularities into the  $D_4^{ij}$  singularities. The decay from the  $D_4$  to the  $A_3$  singularities are proven in section 4.2.1. The mutations  $D_5^{ij} \rightarrow A_4^i$  and  $D_5^{ij} \rightarrow A_4^j$  follow directly since the shell-crossing of the  $D_5^{ij}$  caustic is analogous to the shell-crossing condition on the  $A_4^i$  and  $A_4^j$  caustics.

## 7.2 Singularity transformations

The principal family of singularities – principal in terms of rate of occurrence and spatial dominance – is the  $A$ -family. They are induced by singularities in the geometric structure of one of the eigenvalue fields. In physical terms, they involve one-dimensional collapse on to the emerging singularity. Of a more challenging nature within the evolutionary unfolding of the patterns emerging in fluid flow is the formation of the  $D$ -family of singularities. They occur when two fold sheets corresponding to different eigenvalue fields intersect. Amongst others, this means that the  $D$  singularities connect  $A$  singularities corresponding to two eigenvalue fields.

### 7.2.1 Evolving $A$ -family caustics

The most prominent and abundant singularities are those of the two-dimensional fold sheets  $A_2^i(t)$ . In Eulerian space, they mark the regions where mass elements are turned inside out as the density attains infinity. This happens while they represent the locations where separate matter streams are crossing each other. As time proceeds, the fold sheets  $A_2^i(t)$  sweep over an increasingly larger Lagrangian region. Ultimately, integrating over time, they mark an entire Lagrangian volume, which is labelled as  $A_2^i$ . The  $A_2^i$  set forms a three-dimensional variety.

When we wish to identify where a particular individual fold sheet is born, we turn to the cusp points  $A_3^{i+}$ . They are the points on the fold sheets where the corresponding eigenvalue field attains an extremum. Because of this, they mark the sites of birth of the fold singularities. As the  $A_2^i(t)$  sheets unfold, at the edges their surface gets wrapped in a higher order singularity, the cusp curves  $A_3^i(t)$ . In time, these curves move through space and trace out cusp sheets  $A_3^i$ . In the context of the Megaparsec scale matter distribution in the Universe, the cusp sheets are to be associated with the walls or membranes in the cosmic web [3, 14, 22, 52, 67].

A dynamically interesting process occurs at the cusp points  $A_3^{i-}$ , which are the saddle points of the corresponding eigenvalue field  $\mu_{ti}$  that at a given time are encapsulated by the fold sheet  $A_2^i$ . At the  $A_3^{i-}$  points, we see the merging or annihilation of fold sheets  $A_2^i$  into a larger structure (cf. figure 4). Mathematically, they mark the key locations where the topology of the eigenvalue field changes abruptly. Physically, they are associated with the merging of separate structural components, a manifestation of the hierarchical buildup of structural complexity [22, 67].

Also the cusp curves  $A_3^i(t)$  can get folded. In Eulerian space, the folding of the cusp curves manifests itself as  $A_4^i(t)$  swallowtail points. As time proceeds, these points move through space and define the swallowtail curve  $A_4^i$ . It is of interest to note that the swallowtail curve is embedded in the cusp sheet, i.e.  $A_4^i \subset A_3^i$ . In the context of the cosmic structure formation process, the swallowtail curves outline and trace perhaps the most outstanding feature of the cosmic web, the pronounced elongated filaments that form the spine of the weblike network [3, 22, 67].

Also these features build up in a hierarchical process of small filaments merging into ever larger and more prominent arteries. In the context of the evolving singularity structure that we study, this process is represented by the  $A_4^{i+}$  points and  $A_4^{i-}$  points. They define the decisive junctions where significant changes in topology occur. For the  $A_4^{i\pm}$  points this concerns their identity in the gradient of the eigenvalue field, in which the  $A_4^{i+}$  are maxima

and minima and  $A_4^{i-}$  points are the saddle points. The implication of this is that cusp curves get created or annihilated at  $A_4^{i+}$  points, while they merge or separate at  $A_4^{i-}$  points.

The final morphological constituent in this structural hierarchy of singularities is that of the butterfly points  $A_5^i$ . They conclude the  $A$ -family of singularities, i.e. the family of singularities that correspond to the spatial characteristics of the field of one eigenvalue  $\mu_i$ . The swallowtail curves  $A_4^i$  get folded at  $A_5^i$  butterfly points. In the three-dimensional structural pattern that formed in the fluid, these will represent nodes. In the cosmic web, they define the nodal junctions, connecting to the various filamentary extensions that outline its spine [3, 14, 22, 25, 67]. In principle, for a given initial field and dynamical evolution, one might use these identifications to e.g. evaluate how many filaments are connected to the network nodes [4, 57].

### 7.2.2 Evolving $D$ -family caustics

The  $A_2^i(t)$  and  $A_2^j(t)$  sheets, with  $i \neq j$ , intersect in the elliptic and hyperbolic umbilic points  $D_4^{\pm ij}(t)$ . In contrast to the  $A$  family of singularities, the collapse into  $D$  singularities is two-dimensional. It leads to the birth of the so-called *umbilic* points. Over time, they trace out the umbilic curve  $D_4^{\pm ij}$ . The collapse process may occur in two distinctive ways, indicated by the labels + and -.

The topology of the variety  $D_4^{\pm ij}(t)$  changes at  $D_4^{ij\pm}$  and  $D_5$  points. An interesting characteristic of umbilic curves is that they are always created or annihilated in pairs. The  $D_4^{ij\pm}$  points correspond to the creation or annihilation of two  $D_4^{\pm ij}$  curves of the same signature. By contrast, the  $D_5^{ij}$  points correspond to the creation or annihilation of a pair with one  $D_4^{+ij}$  and one  $D_4^{-ij}$  point.

## 8 Discussion & Conclusions

In this study we have developed a general formalism for identifying the caustic structure of a dynamically evolving mass distribution, in an arbitrary dimensional space. Through a new and direct derivation of the caustic conditions for the classification and characterization of singularities that will form in an evolving matter field, our study enables the practical implementation of a toolset for identifying the spatial location and outline of each relevant class of emerging singularities. By enabling the development of such instruments, and the application of these to any cosmological primordial density and velocity field, our study opens the path towards further insight into the dynamics of the formation and evolution of the morphological features populating the cosmic web. In particular significant is that it will enable us to obtain a fundamental understanding of the spatial organization of the cosmic web, i.e. of the way in which these structural components are arranged and connected.

Caustics are prominent features emerging in advanced stages of dynamically evolving fluids. They mark the positions where fluid elements cross and multi-stream regions form. They are associated with regions of infinite density, and often go along with the formation of shocks. In the context of the gravitationally evolving mass distribution in the universe, caustics emerge in regions in which nonlinear gravitational collapse starts to take place. As such, they are a typical manifestation of the structure formation process at the stage where it transits from the initial linear evolution to that of more advanced nonlinear configurations involving gravitational contraction and collapse. The overall spatial organization of matter at the corresponding scale is that of the cosmic web, which assembles flattened walls, elongated

filaments and tendrils and dense, compact cluster nodes in an intricate multiscale weblike network that pervades the Universe.

Over the past decades our understanding of the formation and evolution of the cosmic web has advanced considerably. The availability of large computer simulations have been instrumental in this, as they enabled us to follow the cosmic structure formation process in detail (see e.g. [60, 65, 70]). In combination with new theoretical insights [14, 67], this has led to the development of a general picture of the emergence of the weblike matter and galaxy distribution. The full phase-space dynamics of the process and its manifestation in the emerging matter distribution is an instrumental aspect of this that only recently received more prominent attention. While the study by Zel'dovich [73] already underlined the importance of a full phase-space description for understanding cosmic structure formation (see also [63, 64]), with the exception of a few prominent studies [10] the wealthy information content of full 6-D phase-space escaped attention.

A series of recent publications initiated a resurgence of interest in the phase-space aspects of the cosmic structure formation process. They realized that the morphology of components in the evolving matter distribution is closely related to its multistream character [1, 30, 54, 58, 62] (for an early study on this observation see [20]). This realization is based on the recognition that the emergence of nonlinear structures occurs at locations where different streams of the corresponding flow field cross each other. Looking at the appearance of the evolving spatial mass distribution as a 3D *phase space sheet* folding itself in 6D phase space, this establishes a connection between the structure formation process and the morphological classification of the emerging structure. Moreover, to further our understanding of the dynamical evolution and buildup of the cosmic matter distribution, we also need to answer the question in how far the various emerging structural features connect up in the overall weblike network of the cosmic web.

To be able to answer the questions, we study the emergence of singularities and caustics in a dynamically evolving mass distribution. Our analysis is built on the seminal work by Arnol'd, specifically his classification of singularities in Lagrangian catastrophe theory. In a three-dimensional setting we can recognize two series of singularities, the  $A_k$  and  $D_k$  series. The 4 classes of  $A_k$  singularities -  $A_2$ ,  $A_3$ ,  $A_4$  and  $A_5$  - are the singularities for which the caustic condition holds for one eigenvalue. The  $D$ -family of umbilic singularities - including the  $D_4^+$ ,  $D_4^-$  and  $D_5$  - are caustic for which the caustic conditions are satisfied by two eigenvalue simultaneously. In three-dimensional fluids, the case in which all three eigenvalues simultaneously satisfy the caustic conditions, the  $E$ -family caustics, is non-degenerate.

One important aspect of our study is the definition of an alternative and more straightforward derivation of *caustic conditions*. These conditions consist of a logical sequence of straightforward mathematical expressions involving both the *eigenvalues* and *eigenvectors* of the deformation tensor field of an evolving matter field. The conditions are derived for Lagrangian catastrophe theory, and as such are restricted to Hamiltonian dynamics. The derived conditions are valid for generic fluids, and also allow for the systems that include dissipative terms and vorticity.

On the basis of the derived formalism, we show how the caustics of a Lagrangian fluid form an intricate skeleton of the nonlinear evolution of the fluid. The family of newly derived caustic conditions allow a significant extension and elaboration of the work described in Arnold et al. (1982) [10]. They classified the caustics that develop in one- and two-dimensional systems that evolve according to the Zel'dovich approximation. While [8] did offer a qualitative description of caustics in the three-dimensional situation, this did not materialize in a prac-

tical application to the full three-dimensional cosmological setting. The expressions derived in our study, and the specific identification of the important role of the deformation tensor eigenvectors, have enabled us to breach this hiatus. To identify the full spatial distribution and arrangement of caustics in the evolving three-dimensional cosmic matter distribution, we follow the philosophy exposed in the two-dimensional study by Hidding et al. 2014 [31, 39]. By relating the singularity distribution to the spatial properties of the initial Gaussian deformation field, [39] managed to identify and show the spatial connectivity of singularities and establish how in a hierarchical evolutionary sequence they evolve and may ultimately merge with surrounding structures.

When applied to the Zel'dovich approximation for cosmic structure formation, the caustic conditions form a skeleton of the caustic web. In the context of the cosmic web, we may identify these singularities with different components in the cosmic web. This observation by itself leads to some radically new insights into the origin of the structural features in the cosmic web. The  $A_3$  cusp singularities are related to the *walls* of the skeleton of the cosmic web. The  $A_4$  swallowtail singularities trace the filamentary ridges and tendrils in the cosmic web. Also the  $D_4^\pm$  hyperbolic and elliptic umbilic singularities are related to the filamentary spine of the spine, as they define the dense filamentary extensions of the cluster nodes. The butterfly ( $A_5$ ) and parabolic umbilic ( $D_5$ ) singularities are both connected with the nodes of the weblike pattern. One immediate observation of considerable interest is that the line-like  $A_4$  and  $D_4^\pm$  features trace the connectivity of the cosmic web in meticulous detail. Perhaps equally or even more interesting, and of key importance for our understanding of the dynamical evolution of the cosmic web, is the observation that both filaments and tendrils, as well as nodes, may have formed due to the folding by the phase-space sheet induced by only one deformation eigenvalue: the filamentary  $A_4$  caustics and nodal  $A_5$  caustic belong to the one eigenvalue  $A$  family of caustics. In other words, collapse along the second eigenvector is not necessary to create a filament-like structure, and not even collapse along both second and third eigenvector is needed for the appearance of nodes (see [39, 40]). This insight leads to a radical new insight on structure formation, in that it suggests the existence of different possible late-time morphologies for filaments and nodes [40].

A realization of key importance emanating from our work is that it is not sufficient to limit a structural analysis to the eigenvalues of the deformation tensor field. Usually neglected, we argue – and show by a few examples – that it is necessary to include the information contained in the (local) deformation tensor eigenvectors, our study has demonstrated and emphasized that for the identification of the full spatial outline of the cosmic web's skeleton. In an accompanying numerical study of the caustic skeleton in cosmological  $N$ -body simulations, we illustrate how essential it is to invoke the deformation eigenvectors in the analysis [32]. This study will present a numerical and statistical comparison between the matter distribution in the simulation and the caustic skeleton of the three-dimensional cosmic web.

Amongst the potentially most important products of the current project is the fact that the caustic skeleton inferred from the Zel'dovich approximation adheres closely to the spine of the full nonlinear matter distribution. The direct implication is that we may directly link the outline of the cosmic web to the initial Gaussian density and velocity field. On the basis of the corresponding deformation field, one may then expect it to be possible to calculate a range of properties analytically. The fact that we may invoke Gaussian statistics facilitates the calculation of a wide range of geometric and topological characteristics of the cosmic web, as they are directly related to the primordial Gaussian deformation field, its eigenvalues and eigenvectors. The first step towards this program were taken by [33]. A few examples

of results of such a statistical treatment for 2-dimensional fluids are described in [31]. It describes how one may not only analytically compute the distribution of maxima, or minima, but also the population of singularities and the length of caustic lines. This will represent a major extension of statistical descriptions that were solely based on the eigenvalue fields (see e.g. [29, 57]). Moreover, the ability to infer solid analytical results for a range of parameters quantifying the cosmic web will be a key towards identifying properties of the cosmic web that are sensitive to the underlying cosmology. This, in turn, would enable the use of these properties to infer cosmological parameters, investigate the nature of dark matter and dark energy, trace the effects of deviations from standard gravity, and other issues of general cosmological interest.

Notwithstanding the observation that the caustic skeleton inferred from the Zel'dovich approximation appears to closely adhere to the full nonlinear structure seen in  $N$ -body simulations, an aspect that still needs to be addressed in detail is the influence of the dynamical evolution on the developing caustic structure. This concerns in particular the description of the dynamics of the system. Given the nature of singularities, the process of caustic formation might be very sensitive to minor deviations of the mass element deformations and hence the modelling of the dynamics. This may even strongly affect the predicted population of caustics and their spatial organization in the skeleton of the cosmic web. The Zel'dovich formalism [73] is a first-order Lagrangian approximation. A range of studies have shown that second order Lagrangian descriptions, often named 2LPT, provide a considerably more accurate approximation of in particular the mildly nonlinear phases that are critical for understanding the cosmic web [15, 17, 19, 20, 61]. In addition to a follow-up study in which we explore the caustic structure according to 2LPT and possible systematic differences with that predicated by the Zel'dovich approximation, we will also systematically investigate the caustic skeleton in the context of the adhesion formalism [35, 36, 38, 41]. Representing a fully nonlinear extension of the Zel'dovich formalism through the inclusion of an effective gravitational interaction term for the emerging structures, it is capable of following the hierarchical buildup of structure. While it provides a highly insightful model for the hierarchically evolving cosmic web, it also affects the flow patterns and hence the multistream structure in the cosmic mass distribution. In how far this will affect the caustic skeleton remains a major question for our work.

Finally, of immediate practical interest to our project will be identification of the various classes of singularities that are populating the Local Universe. On the basis of advanced Bayesian reconstruction techniques, various groups have been able to infer constrained realizations of the implied Gaussian primordial density and velocity field in a given cosmic volume [44, 45, 50, 51]. From these constrained initial density and deformation fields, we may subsequently determine the caustic structure in the Local Universe (see e.g. [40]). The resulting caustic skeleton of the local cosmic web may then be confronted with the structures – clusters, groups and galaxies – that surveys have observed. Ultimately, this will enable us to reconstruct the cosmic history of objects and structures in the local Universe.

In summary, the ability to relate the formation and hierarchical evolution of structure in the Universe to the tale of the emergence and fate of singularities in the cosmic density field provides the basis for a dynamical theory for the development of the cosmic web, including that of its substructure. This will be the principal question and subject of the sequel to the work that we have presented here.

## Acknowledgements

We thank Sergei Shandarin for having raised our interest in caustics as a key towards the dynamical understanding of the cosmic web. We are grateful to Bernard Jones, Adi Nusser, Neil Turok, and Gert Vegter for many useful and encouraging discussions. JF acknowledges the Perimeter Institute for facilitating this research through the support by the Government of Canada through the Department of Innovation, Science and Economic Development Canada and by the Province of Ontario through the Ministry of Research, Innovation and Science.

## References

- [1] T. Abel, O. Hahn, and R. Kaehler. Tracing the dark matter sheet in phase space. *Mon. Not. R. Astron. Soc.*, 427:61–76, November 2012.
- [2] R. J. Adler. *The Geometry of Random Fields*. 1981.
- [3] M. A. Aragón-Calvo, E. Platen, R. van de Weygaert, and A. S. Szalay. The Spine of the Cosmic Web. *Astrophys. J.*, 723:364–382, November 2010.
- [4] M. A. Aragón-Calvo, R. van de Weygaert, and B. J. T. Jones. Multiscale phenomenology of the cosmic web. *Mon. Not. R. Astron. Soc.*, 408:2163–2187, November 2010.
- [5] V. I. Arnol'd. Normal forms for functions near degenerate critical points, the Weyl groups of  $A_k, D_k, E_k$  and Lagrangian singularities. *Functional Anal. Appl.*, 6:1972, 1972.
- [6] V. I. Arnol'd. Wave front evolution and equivalent Morse lemma. *Communications in Pure Applied Mathematics*, 29:557–582, November 1976.
- [7] V. I. Arnol'd. *Mathematical methods of classical mechanics*. 1978.
- [8] V. I. Arnol'd. Evolution of singularities of potential flows in collisionless media and transformations of caustics in three-dimensional space. *Trudy Seminar imeni G Petrovskogo*, 8:21–57, 1982.
- [9] V. I. Arnol'd and B. A. Khesin. Topological methods in hydrodynamics. *Annual Review of Fluid Mechanics*, 24:145–166, 1992.
- [10] V. I. Arnol'd, S. F. Shandarin, and I. B. Zel'dovich. The large scale structure of the universe. I - General properties One- and two-dimensional models. *Geophysical and Astrophysical Fluid Dynamics*, 20:111–130, 1982.
- [11] V.I. Arnol'd, S.M. Gusein-Zade, and A.N. Varchenko. *Singularities of Differentiable Maps, Volume 2: Monodromy and Asymptotics of Integrals*. Modern Birkhäuser Classics. Birkhauser Boston, 2012.
- [12] V.I. Arnol'd, A. Varchenko, and S.M. Gusein-Zade. *Singularities of Differentiable Maps: Volume I: The Classification of Critical Points Caustics and Wave Fronts*. Monographs in Mathematics. Birkhauser Boston, 2012.
- [13] J. M. Bardeen, J. R. Bond, N. Kaiser, and A. S. Szalay. The statistics of peaks of Gaussian random fields. *The Astrophysical Journal*, 304:15–61, May 1986.
- [14] J. R. Bond, L. Kofman, and D. Pogosyan. How filaments of galaxies are woven into the cosmic web. *Nature*, 380:603–606, April 1996.
- [15] F. R. Bouchet, S. Colombi, E. Hivon, and R. Juszkiewicz. Perturbative Lagrangian approach to gravitational instability. *Astron. Astrophys.*, 296:575, April 1995.
- [16] J.W. Bruce. A classification of 1-parameter families of map germs  $r^3, 0 \rightarrow r^3, 0$  with applications to condensation problems. *J. Lond. Math. Soc.*, II. Ser. 30(2):375–384, 1985.

- [17] T. Buchert. Lagrangian theory of gravitational instability of Friedman-Lemaitre cosmologies and the 'Zel'dovich approximation'. *Mon. Not. R. Astron. Soc.*, 254:729–737, February 1992.
- [18] T. Buchert. Lagrangian perturbation theory - A key-model for large-scale structure. *Astron. Astrophys.*, 267:L51–L54, January 1993.
- [19] T. Buchert. Lagrangian Theory of Gravitational Instability of Friedman-Lemaitre Cosmologies - a Generic Third-Order Model for Nonlinear Clustering. *Mon. Not. R. Astron. Soc.*, 267:811, April 1994.
- [20] T. Buchert and J. Ehlers. Lagrangian theory of gravitational instability of Friedman-Lemaitre cosmologies – second-order approach: an improved model for non-linear clustering. *Mon. Not. R. Astron. Soc.*, 264, September 1993.
- [21] T. Buchert, A. L. Melott, and A. G. Weiss. Testing higher-order Lagrangian perturbation theory against numerical simulations I. Pancake models. *Astron. Astrophys.*, 288:349–364, August 1994.
- [22] M. Cautun, R. van de Weygaert, B. J. T. Jones, and C. S. Frenk. Evolution of the cosmic web. *Mon. Not. R. Astron. Soc.*, 441:2923–2973, July 2014.
- [23] M. S. Chong, A. E. Perry, and B. J. Cantwell. A general classification of three-dimensional flow fields. *Physics of Fluids*, 2:765–777, May 1990.
- [24] J. M. Colberg, K. S. Krughoff, and A. J. Connolly. *Mon. Not. R. Astron. Soc.*, 359:272, 2005.
- [25] J. M. Colberg, K. S. Krughoff, and A. J. Connolly. Intercluster filaments in a  $\Lambda$ CDM Universe. *Mon. Not. R. Astron. Soc.*, 359:272–282, May 2005.
- [26] M. Colless and et. al. The 2dF Galaxy Redshift Survey: Final Data Release. *ArXiv Astrophysics e-prints*, June 2003.
- [27] P. Creminelli, A. Nicolis, L. Senatore, M. Tegmark, and M. Zaldarriaga. Limits on non-Gaussianities from WMAP data. *Journal of Cosmology and Astroparticle Physics*, 5:004, May 2006.
- [28] T. Delmarcelle. *The Visualization of Second-Order Tensor Fields*. PhD thesis, STANFORD UNIVERSITY., 1995.
- [29] A. G. Doroshkevich. Spatial structure of perturbations and origin of galactic rotation in fluctuation theory. *Astrophysics*, 6:320–330, October 1970.
- [30] B. L. Falck, M. C. Neyrinck, and A. S. Szalay. ORIGAMI: Delineating Halos Using Phase-space Folds. *Astrophys. J.*, 754:126, August 2012.
- [31] J. Feldbrugge, J. Hidding, and R. van de Weygaert. Statistics of Caustics in Large-Scale Structure Formation. *Proceedings of IAU Symposium 308 “The Zeld’ovich Universe: Genesis and Growth of the Cosmic Web”*, December 2014.
- [32] J. Feldbrugge, J. Hidding, and R. van de Weygaert. In preparation. *Mon. Not. R. Astron. Soc.*, 2017.
- [33] Job Feldbrugge. Statistics of caustics in large-scale structure formation. Master's thesis, Rijksuniversiteit Groningen, the Netherlands, 2014.
- [34] H. Goldstein. *Classical Mechanics*. Addison-Wesley, 1980.
- [35] S. N. Gurbatov, A. I. Saichev, and S. F. Shandarin. The large-scale structure of the universe in the frame of the model equation of non-linear diffusion. *Mon. Not. R. Astron. Soc.*, 236:385–402, January 1989.
- [36] S. N. Gurbatov, A. I. Saichev, and S. F. Shandarin. Large-scale structure of the Universe. The Zeldovich approximation and the adhesion model. *Physics Uspekhi*, 55:223–249, March 2012.

- [37] L. Guzzo, M. Scodéglio, B. Garilli, B. R. Granett, A. Fritz, U. Abbas, C. Adami, S. Arnouts, J. Bel, M. Bolzonella, D. Bottini, E. Branchini, A. Cappi, J. Coupon, O. Cucciati, I. Davidzon, G. De Lucia, S. de la Torre, P. Franzetti, M. Fumana, P. Hudelot, O. Ilbert, A. Iovino, J. Krywult, V. Le Brun, O. Le Fèvre, D. Maccagni, K. Malek, F. Marulli, H. J. McCracken, L. Paioro, J. A. Peacock, M. Polletta, A. Pollo, H. Schlagenhaufner, L. A. M. Tasca, R. Tojeiro, D. Vergani, G. Zamorani, A. Zanichelli, A. Burden, C. Di Porto, A. Marchetti, C. Marinoni, Y. Mellier, L. Moscardini, R. C. Nichol, W. J. Percival, S. Phleps, and M. Wolk. The VIMOS Public Extragalactic Redshift Survey (VIPERS). An unprecedented view of galaxies and large-scale structure at  $0.5 < z < 1.2$ . *Astron. Astrophys.*, 566:A108, June 2014.
- [38] J.. Hidding. *The Phase-Space Geometry of the Cosmic Web*, Ph.D. thesis, University of Groningen, 2018.
- [39] J. Hidding, S. F. Shandarin, and R. van de Weygaert. The Zel'dovich approximation: key to understanding cosmic web complexity. *Mon. Not. R. Astron. Soc.*, 437:3442–3472, February 2014.
- [40] J. Hidding, R. van de Weygaert, and S. Shandarin. The Zeldovich & Adhesion approximations and applications to the local universe. In R. van de Weygaert, S. Shandarin, E. Saar, and J. Einasto, editors, *The Zeldovich Universe: Genesis and Growth of the Cosmic Web*, volume 308 of *IAU Symposium*, pages 69–76, October 2016.
- [41] J. Hidding, R. van de Weygaert, G. Vegter, B. J. T. Jones, and M. Teillaud. The Sticky Geometry of the Cosmic Web. *ArXiv e-prints*, May 2012.
- [42] J. P. Huchra, L. M. Macri, K. L. Masters, T. H. Jarrett, P. Berlind, M. Calkins, A. C. Crook, R. Cutri, P. Erdođu, E. Falco, T. George, C. M. Hutcheson, O. Lahav, J. Mader, J. D. Mink, N. Martimbeau, S. Schneider, M. Skrutskie, S. Tokarz, and M. Westover. The 2MASS Redshift Survey-Description and Data Release. *ApJS*, 199:26, April 2012.
- [43] V. Icke. *Astron. Astrophys.*, 27:1, 1973.
- [44] J. Jasche, F. S. Kitaura, C. Li, and T. A. Enßlin. Bayesian non-linear large-scale structure inference of the Sloan Digital Sky Survey Data Release 7. *Mon. Not. R. Astron. Soc.*, 409:355–370, November 2010.
- [45] F.-S. Kitaura. The initial conditions of the Universe from constrained simulations. *Mon. Not. R. Astron. Soc.*, 429:L84–L88, February 2013.
- [46] E. Komatsu, A. Kogut, M. R. Nolta, C. L. Bennett, M. Halpern, G. Hinshaw, N. Jarosik, M. Limon, S. S. Meyer, L. Page, D. N. Spergel, G. S. Tucker, L. Verde, E. Wollack, and E. L. Wright. First-Year Wilkinson Microwave Anisotropy Probe (WMAP) Observations: Tests of Gaussianity. *The Astrophysical Journal Supplement*, 148:119–134, September 2003.
- [47] I. A. Kravtsov and I. I. Orlov. Caustics, catastrophes, and wave fields. *Uspekhi Fizicheskikh Nauk*, 141:591–627, December 1983.
- [48] L.D. Landau and E.M. Lifshitz. *Volume 1: Mechanics*. Pergamom, 1959.
- [49] L.D. Landau and E.M. Lifshitz. *Volume 6: Fluid Mechanics*. Butterworth-Heinemann, 1976.
- [50] F. Leclercq, J. Jasche, G. Lavaux, B. Wandelt, and W. Percival. The phase-space structure of nearby dark matter as constrained by the SDSS. *Journal of Cosmology and Astroparticle Physics*, 6:049, June 2017.
- [51] F. Leclercq, J. Jasche, and B. Wandelt. Bayesian analysis of the dynamic cosmic web in the SDSS galaxy survey. *Journal of Cosmology and Astroparticle Physics*, 6:015, June 2015.
- [52] N. I Libeskind, R. van de Weygaert, M. Cautun, B. Falck, E. Tempel, T. Abel, M. Alpaslan, M. A. Aragoon-Calvo, J. E. Forero-Romero, R. Gonzalez, S. Gottlober, O. Hahn, W. A. Hellwing, Y. Hoffman, B. J. T. Jones, F. Kitaura, A. Knebe, S. Manti, M. Neyrinck, S. E. Nuza,

- N. Padilla, E. Platen, N. Ramachandra, A. Robotham, E. Saar, S. Shandarin, M. Steinmetz, R. S. Stoica, T. Sousbie, and G. Yepes. Tracing the cosmic web. *ArXiv e-prints*, May 2017.
- [53] P. J. Morrison. Hamiltonian description of the ideal fluid. *Reviews of Modern Physics*, 70:467–521, April 1998.
- [54] M. C. Neyrinck. Origami constraints on the initial-conditions arrangement of dark-matter caustics and streams. *ArXiv e-prints*, February 2012.
- [55] P. J. E. Peebles. *The large-scale structure of the universe*. 1980.
- [56] Planck Collaboration, P. A. R. Ade, N. Aghanim, M. Arnaud, F. Arroja, M. Ashdown, J. Aumont, C. Baccigalupi, M. Ballardini, A. J. Banday, and et al. Planck 2015 results. XVII. Constraints on primordial non-Gaussianity. *Astron. Astrophys.*, 594:A17, September 2016.
- [57] D. Pogosyan, C. Pichon, C. Gay, S. Prunet, J. F. Cardoso, T. Sousbie, and S. Colombi. The local theory of the cosmic skeleton. *Mon. Not. R. Astron. Soc.*, 396:635–667, June 2009.
- [58] Nesar S. Ramachandra and Sergei F. Shandarin. Multi-stream portrait of the cosmic web. *Monthly Notices of the Royal Astronomical Society*, 452(2):1643–1653, 2015.
- [59] R. Salmon. Hamiltonian fluid mechanics. *Annual Review of Fluid Mechanics*, 20:225–256, 1988.
- [60] J. Schaye, R. A. Crain, R. G. Bower, M. Furlong, M. Schaller, T. Theuns, C. Dalla Vecchia, C. S. Frenk, I. G. McCarthy, J. C. Helly, A. Jenkins, Y. M. Rosas-Guevara, S. D. M. White, M. Baes, C. M. Booth, P. Camps, J. F. Navarro, Y. Qu, A. Rahmati, T. Sawala, P. A. Thomas, and J. Trayford. The EAGLE project: simulating the evolution and assembly of galaxies and their environments. *Mon. Not. R. Astron. Soc.*, 446:521–554, January 2015.
- [61] R. Scoccimarro. Gravitational Clustering from  $\chi^2$  Initial Conditions. *Astrophys. J.*, 542:1–8, October 2000.
- [62] S. Shandarin, S. Habib, and K. Heitmann. Cosmic web, multistream flows, and tessellations. *Phys. Rev. D*, 85(8):083005, April 2012.
- [63] S. F. Shandarin and R. A. Sunyaev. The conjecture of the cosmic web. Commentary on: Zel'dovich Ya. B., 1970, A&A, 5, 84. *A&A*, 500:19–20, June 2009.
- [64] S. F. Shandarin and Y. B. Zel'dovich. The large-scale structure of the universe: Turbulence, intermittency, structures in a self-gravitating medium. *Reviews of Modern Physics*, 61:185–220, April 1989.
- [65] V. Springel, S. D. M. White, A. Jenkins, C. S. Frenk, N. Yoshida, L. Gao, J. Navarro, R. Thacker, D. Croton, J. Helly, J. A. Peacock, S. Cole, P. Thomas, H. Couchman, A. Evrard, J. Colberg, and F. Pearce. Simulations of the formation, evolution and clustering of galaxies and quasars. *Nature*, 435:629–636, June 2005.
- [66] M. Tegmark, M. R. Blanton, M. A. Strauss, F. Hoyle, D. Schlegel, R. Scoccimarro, M. S. Vogeley, D. H. Weinberg, I. Zehavi, A. Berlind, T. Budavari, A. Connolly, D. J. Eisenstein, D. Finkbeiner, J. A. Frieman, J. E. Gunn, A. J. S. Hamilton, L. Hui, B. Jain, D. Johnston, S. Kent, H. Lin, R. Nakajima, R. C. Nichol, J. P. Ostriker, A. Pope, R. Scranton, U. Seljak, R. K. Sheth, A. Stebbins, A. S. Szalay, I. Szapudi, L. Verde, Y. Xu, J. Annis, N. A. Bahcall, J. Brinkmann, S. Burles, F. J. Castander, I. Csabai, J. Loveday, M. Doi, M. Fukugita, J. R. Gott, III, G. Hennessy, D. W. Hogg, Ž. Ivezić, G. R. Knapp, D. Q. Lamb, B. C. Lee, R. H. Lupton, T. A. McKay, P. Kunszt, J. A. Munn, L. O'Connell, J. Peoples, J. R. Pier, M. Richmond, C. Rockosi, D. P. Schneider, C. Stoughton, D. L. Tucker, D. E. Vanden Berk, B. Yanny, D. G. York, and SDSS Collaboration. The Three-Dimensional Power Spectrum of Galaxies from the Sloan Digital Sky Survey. *Astrophys. J.*, 606:702–740, May 2004.
- [67] R. van de Weygaert and J. R. Bond. Clusters and the Theory of the Cosmic Web. In M. Plionis, O. López-Cruz, and D. Hughes, editors, *A Pan-Chromatic View of Clusters of*

*Galaxies and the Large-Scale Structure*, volume 740 of *Lecture Notes in Physics, Berlin Springer Verlag*, page 335, 2008.

- [68] V. A. Vasil'ev. Asymptotic exponential integrals, Newton's diagram, and the classification of minimal points. *Plenum Publishing Corporation*, 1978.
- [69] M. Vergassola, B. Dubrulle, U. Frisch, and A. Noullez. Burgers' equation, Devil's staircases and the mass distribution for large-scale structures. *Astron. Astrophys.*, 289:325–356, September 1994.
- [70] M. Vogelsberger, S. Genel, V. Springel, P. Torrey, D. Sijacki, D. Xu, G. Snyder, D. Nelson, and L. Hernquist. Introducing the Illustris Project: simulating the coevolution of dark and visible matter in the Universe. *Mon. Not. R. Astron. Soc.*, 444:1518–1547, October 2014.
- [71] X. Wang, A. Szalay, M. A. Aragón-Calvo, M. C. Neyrinck, and G. L. Eyink. Kinematic Morphology of Large-scale Structure: Evolution from Potential to Rotational Flow. *Astrophys. J.*, 793:58, September 2014.
- [72] I. B. Zeldovich, A. V. Mamaev, and S. F. Shandarin. Laboratory observation of caustics, optical simulation of the motion of particles, and cosmology. *Uspekhi Fizicheskikh Nauk*, 139:153–163, January 1983.
- [73] Y. B. Zel'dovich. Gravitational instability: An approximate theory for large density perturbations. *A&A*, 5:84–89, March 1970.

## A Zel'dovich approximation

The Zel'dovich approximation is the first order approximation of a Lagrangian pressureless fluid evolving under self gravity, [73]. The Zel'dovich approximation is the simplest example of a Lagrangian fluid with Hamiltonian dynamics and serves as a good illustration of the caustic conditions. The displacement map of the Zel'dovich approximation factors into a term depending on time and a term depending on the initial conditions

$$s_t(q) = -b_+(t)\nabla_q\Psi(q), \quad (\text{A.1})$$

with the linearized velocity potential  $\Psi(q)$  and growing mode  $b_+(t)$ . The growing mode can be obtained from linear Eulerian perturbation theory. Up to linear order, the linearized velocity potential is proportional to the linearly extrapolated gravitational potential at the current epoch  $\phi_0(q)$ , i.e.

$$\Psi(q) = \frac{2}{3\Omega_0 H_0^2} \phi_0(q), \quad (\text{A.2})$$

with current Hubble constant  $H_0$  and current energy density  $\Omega_0$ . The linearized velocity potential  $\Psi(q)$  encodes the initial conditions while the growing mode  $b_+(t)$  encodes the cosmological evolution of the fluid. For the Zel'dovich approximation it is common to define the deformation tensor as

$$\psi_{ij} = \frac{\partial^2 \Psi(q)}{\partial q_i \partial q_j} \quad (\text{A.3})$$

with eigenvalues  $\lambda_i(q)$  satisfying  $\mu_i(q, t) = -b_+(t)\lambda_i(q)$ . The density in the Zel'dovich approximation can be expressed as

$$\rho(x', t) = \sum_{q \in A(x', t)} \frac{\rho_i(q)}{(1 - b_+(t)\lambda_1(q))(1 - b_+(t)\lambda_2(q))(1 - b_+(t)\lambda_d(q))}, \quad (\text{A.4})$$

with  $\rho_i$  the initial density field. Caustics occur at  $q$  at time  $t$  if and only if

$$\lambda_i(q) = \frac{1}{b_+(t)} \quad (\text{A.5})$$

for at least one  $i$ . The eigenvalues  $\lambda_i$  are functions determined by the initial gravitational field. Equation (A.5) can be pictured as a hyperplane at height  $1/b_+(t)$ . The intersection of this plane with the graph of the eigenvalues undergoes shell-crossing at that time. For the Zel'dovich approximation the caustic conditions in terms of the eigenvalues  $\lambda_i$  are given by

$$A_1 = \{q \in L | \lambda_i(q) \neq 1/b_+(t) \text{ for all } t \text{ and } i\}, \quad (\text{A.6})$$

$$A_2^i(t) = \{q \in L | \lambda_i(q) = 1/b_+(t)\}, \quad (\text{A.7})$$

$$A_3^i(t) = \{q \in L | q \in A_2^i(t) \text{ and } \lambda_{i,i}(q) = 0\}, \quad (\text{A.8})$$

$$A_4^i(t) = \{q \in L | q \in A_3^i(t) \text{ and } \lambda_{i,ii}(q) = 0\}, \quad (\text{A.9})$$

$$A_5^i(t) = \{q \in L | q \in A_4^i(t) \text{ and } \lambda_{i,iii}(q) = 0\}, \quad (\text{A.10})$$

$$D_4^{\pm ij}(t) = \{q \in L | \lambda_i(q) = \lambda_j(q) = 1/b_+(t) \text{ and } \text{sign}(S_M) = \pm 1\}, \quad (\text{A.11})$$

$$D_5^{ij}(t) = \{q \in L | q \in D_4^{ij}(t) \text{ and } (\lambda_i - \lambda_j)_{,i}(q) = (\lambda_i - \lambda_j)_{,j}(q) = 0\}, \quad (\text{A.12})$$

and the points at which the topology of above sets changes

$$A_3^{i+} = \{q \in L | q \in A_2^i \wedge \lambda_i(q) \text{ max-/minimum of } \lambda_i\}, \quad (\text{A.13})$$

$$A_3^{i-} = \{q \in L | q \in A_2^i \text{ saddle point of } \lambda_i\}, \quad (\text{A.14})$$

$$A_4^{i+} = \{q \in L | q \in A_3^i \wedge \lambda_{i,ii}(q) \text{ max-/minimum of } \lambda_{i,ii}|_{A_2}\}, \quad (\text{A.15})$$

$$A_4^{i-} = \{q \in L | q \in A_3^i \text{ saddle point of } \lambda_{i,ii}|_{A_2}\}, \quad (\text{A.16})$$

$$D_4^{ij\pm} = \{q \in L | q \in D_4^{\pm ij} \wedge \lambda_i(q) = \lambda_j(q) \text{ max-/minimum of } \lambda_i|_{D_4^{\pm ij}} = \lambda_j|_{D_4^{\pm ij}}\}. \quad (\text{A.17})$$

with the direction derivatives  $\lambda_{i,i} = \nabla \lambda_i \cdot v_i$ ,  $\lambda_{i,ii} = \nabla \lambda_{i,i} \cdot v_i$  and  $\lambda_{i,iii} = \nabla \lambda_{i,ii} \cdot v_i$ . Note that the eigenvectors are defined modulo multiplication by a real number and really represent lines.

## B Lagrangian maps and Lagrangian equivalence

We here shortly describe the mathematical background of symplectic manifolds, Lagrangian manifolds and Lagrangian maps. For a detailed description and derivations we refer to [11, 12].

### B.1 Symplectic manifolds and Lagrangian maps

A  $2n$ -dimensional symplectic manifold  $(M, \omega)$  is a smooth  $2n$ -dimensional manifold  $M$ , equipped with a closed nondegenerate bilinear 2-form  $\omega$  called the symplectic form. Symplectic manifolds are always even dimensional for  $\omega$  to be nondegenerate. In Hamiltonian dynamics the symplectic form  $\omega$  can be associated to the Poisson brackets which encodes the dynamics of the theory. A Lagrangian manifold  $L$  of a  $2n$ -dimensional symplectic manifold  $(M, \omega)$  is a  $n$ -dimensional submanifold of  $M$  on which the symplectic form  $\omega$  vanishes. Let  $(B, \pi)$  be a Lagrangian fibration of  $(M, \omega)$ , which is a  $n$ -dimensional manifold with a projection map  $\pi : M \rightarrow B$  for which the fibers  $\pi^{-1}(b)$  are Lagrangian manifolds for all  $b \in B$ .

An example of a symplectic manifold is phase space consisting of position and canonical

momenta  $(q_1, \dots, q_n, p_1, \dots, p_n)$  with the symplectic form  $\omega = \sum_i dq_i \wedge dp_i$ . An example of a Lagrangian fibration is  $\{(q_1, \dots, q_n), \pi\}$  with the projection map  $\pi(q_1, \dots, q_n, p_1, \dots, p_n) = (q_1, \dots, q_n)$ .

Give a symplectic manifold  $(M, \omega)$  with a Lagrangian fibration  $(B, \pi)$  we can for every Lagrangian manifold  $L$  define a Lagrangian map  $(\pi \circ i) : L \rightarrow M \rightarrow B$ , with  $i$  being the inclusion map sending  $L$  into  $M$ . Two Lagrangian maps  $(\pi_1 \circ i_1) : L_1 \rightarrow M_1 \rightarrow B_1$  and  $(\pi_2 \circ i_2) : L_2 \rightarrow M_2 \rightarrow B_2$  are defined to be Lagrangian equivalent if there exist diffeomorphisms  $\sigma, \tau$  and  $\nu$  such that  $\tau \circ i_1 = i_2 \circ \sigma$ ,  $\nu \circ \pi_1 = \pi_2 \circ \tau$  and  $\tau^* \omega_2 = \omega_1$ , or equivalently the diagram below commutes

$$\begin{array}{ccccc} L_1 & \xrightarrow{i_1} & (M_1, \omega_1) & \xrightarrow{\pi_1} & B_1 \\ \sigma \downarrow & & \tau \downarrow & & \nu \downarrow \\ L_2 & \xrightarrow{i_2} & (M_2, \omega_2) & \xrightarrow{\pi_2} & B_2 \end{array}$$

## B.2 Displacement as Lagrangian map

Given a Lagrangian submanifold  $\mathcal{L}$  we can construct a corresponding Lagrangian map. First map the Lagrangian submanifold  $\mathcal{L}$  with the inclusion map  $i : \mathcal{L} \rightarrow \mathcal{C}$  to the corresponding points in phase space  $\mathcal{C}$ , i.e.,  $i : (q, x) \mapsto (q, x)$  for all  $(q, x) \in \mathcal{L}$ . Subsequently map these points to a base manifold  $B$  with the projection map  $\pi : \mathcal{C} \rightarrow B$ . In Lagrangian fluid dynamics it is convenient to pick the Eulerian manifold  $E$  as the base manifold  $B$  and define the projection map as  $\pi : (q, x) \mapsto x$  for all  $(q, x) \in \mathcal{C}$ . As there will always be an exact correspondence between the Lagrangian manifold  $L$  and the Lagrangian submanifold  $\mathcal{L}_t \subset \mathcal{C}$  (there exists a unique point  $x \in E$  such that  $(q, x) \in \mathcal{L}_t$  for every  $q \in L$ ), we can associate the Lagrangian map corresponding to  $\mathcal{L}_t$  with the map  $x_t$ . In summary, the map  $x_t$  corresponds uniquely to a Lagrangian map for fluids with Hamiltonian dynamics.

A Lagrangian map can develop regions in which multiple points in the Lagrangian manifold are mapped to the same point in the base space. The points at which the number of pre-images of the Lagrangian map changes are known as Lagrangian singularities. Lagrangian catastrophe theory classifies the stable singularities, stable with respect to small deformations of  $\mathcal{L}$ , up to Lagrangian equivalence. Lagrangian equivalence is a generalization of equivalence up to coordinate transformations. For a precise definition of Lagrangian equivalence we refer to appendix B.

## B.3 Lagrangian map germs

In catastrophe theory it is important to consider the Lagrangian map at a point. This is achieved by means of Lagrangian germs. Starting with a point  $p \in M$  we can consider Lagrangian functions  $F_i : U_i \rightarrow B$  for  $i = 1, 2$  for small environments  $U_i$  of  $p$  which coincide on the intersection  $U_1 \cap U_2$ . The equivalence classes of such Lagrangian functions are Lagrangian germs. The Lagrange equivalence of Lagrangian maps straightforwardly extends to Lagrange equivalence of Lagrangian germs. These are the equivalence classes used in the classification of stable Lagrangian maps, where a Lagrangian germ is stable if and only if every sufficiently small fluctuation on the germ is Lagrange equivalent to the germ.

$A_1 : x(q, 1) = (q_1, q_2, q_3)$	$1 + \mu_1 = 1$	$1 + \mu_2 = 1$	$1 + \mu_3 = 1$
$A_2 : x(q, 1) = (q_1, q_2, q_3^2)$	$1 + \mu_1 = 1$	$1 + \mu_2 = 1$	$1 + \mu_3 = 2q_3$
			$\mu_{3,3} = 2$
$A_3 : x(q, 1) = (q_1, q_2, q_1q_3 + q_3^3)$	$1 + \mu_1 = 1$	$1 + \mu_2 = 1$	$1 + \mu_3 = 3q_3^2 + q_1$
			$\mu_{3,3} = 6q_3$
			$\mu_{3,33} = 6$
$A_4 : x(q, 1) = (q_1, q_2, q_1q_3 + q_3^4)$	$1 + \mu_1 = 1$	$1 + \mu_2 = 1$	$1 + \mu_3 = q_1 + 4q_3^3$
			$\mu_{3,3} = 12q_3^2$
			$\mu_{3,33} = 24q_3$
			$\mu_{3,333} = 24$
$A_5 : x(q, 1) = (q_1, q_2, q_1q_3 + q_2q_3^2 + q_3^5)$	$1 + \mu_1 = 1$	$1 + \mu_2 = 1$	$1 + \mu_3 = q_1 + 2q_2q_3 + 5q_3^4$
			$\mu_{3,3} = 2q_2 + 20q_3^3$
			$\mu_{3,33} = 60q_3^2$
			$\mu_{3,333} = 120q_3$
			$\mu_{3,3333} = 120$
$A_3^\pm : x(q, 1) = (q_1, q_2, (q_1^2 \pm q_2^2)q_3 + q_3^3)$	$1 + \mu_1 = 1$	$1 + \mu_2 = 1$	$1 + \mu_3 = q_1^2 \pm q_2^2 + 3q_3^2$
			$\mu_{3,3} = 6q_3$
			$\mu_{3,33} = 6$
$A_4^\pm : x(q, 1) = (q_1, q_2, q_1q_3 \pm q_2^2q_3^2 + q_3^4)$	$1 + \mu_1 = 1$	$1 + \mu_2 = 1$	$1 + \mu_3 = q_1 \pm 2q_2^2q_3 + 4q_3^3$
			$\mu_{3,3} = \pm 2q_2^2 + 12q_3^2$
			$\mu_{3,33} = 24q_3$
			$\mu_{3,333} = 24$

**Table 2:** The caustic conditions of the normal forms of the  $A$  singularity classes

#### B.4 Gradient maps

Every Lagrangian germ is Lagrange equivalent to the germ of a gradient map. That is to say, for every Lagrangian map  $l = \pi \circ i : \mathcal{L} \rightarrow \mathcal{C} \rightarrow E$  we can for a point  $(q, x) \in \mathcal{L}$  locally write the map as

$$l(q_1, \dots, q_n, x_1, \dots, x_n) = \left( \frac{\partial S}{\partial q_1}, \frac{\partial S}{\partial q_2}, \dots, \frac{\partial S}{\partial q_n} \right) \quad (\text{B.1})$$

for some function  $S : \mathbb{R}^n \rightarrow \mathbb{R}$ . The corresponding map  $x$  is given by

$$x(q_1, \dots, q_n, t) = \left( \frac{\partial S}{\partial q_1}, \frac{\partial S}{\partial q_2}, \dots, \frac{\partial S}{\partial q_n} \right) \quad (\text{B.2})$$

for some time  $t$ . By writing  $S = \frac{1}{2}q^2 + \Psi$  for  $\Psi : \mathbb{R}^3 \times \mathbb{R} \rightarrow \mathbb{R}$  we obtain

$$x(q, t) = q + \frac{\partial \Psi}{\partial q}, \quad (\text{B.3})$$

with the gradient field

$$s = \frac{\partial \Psi}{\partial q}. \quad (\text{B.4})$$

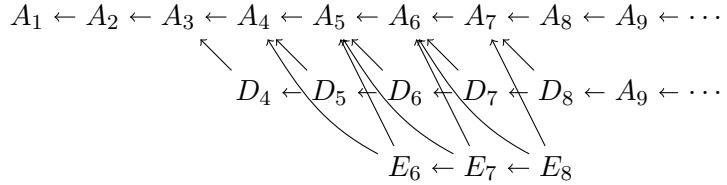
The Jacobian of the displacement map

$$\left[ \frac{\partial s}{\partial q} \right]_{ij} = \frac{\partial^2 \Psi}{\partial q_i \partial q_j} \quad (\text{B.5})$$

is symmetric. The set of eigenvectors  $\{v_i\}$  can be taken to be orthonormal by which the dual vectors coincide with the eigenvectors, i.e.,  $v_i^* = v_i$  for all  $i$ . A Lagrangian map is locally equivalent to the Zel'dovich approximation.

### B.5 Arnol'd's classification of Lagrangian catastrophes

In section 4.1, we described the classification of Lagrangian singularities in up to three dimensions. However the classification extends to higher dimensional singularities. A  $(n+1)$ -dimensional fluid can contain stable singularities in the  $A_i$ ,  $D_i$  and  $E_i$  classes with  $i \leq n+2$ , where the  $D$ -class range starts at  $i=4$  and the  $E$ -class is only defined for  $i=6, 7, 8$ . These singularities decompose into lower-dimensional singularities as illustrated in the unfolding diagram below.



### C Caustic conditions of the normal forms

We here verify the caustic conditions for the normal forms in the generic classification of singularities given in section 5.3. The normal forms of the the Lagrangian singularities given in section 5.4 follow analogously.

The eigenvalue fields and corresponding derivatives in the direction of the eigenvector fields are given in table 2. The eigenvalues of the normal form for the trivial ( $A_1$ ) case equal 1 and thus satisfy the condition  $1 + \mu_i \neq 0$  for all  $i$ . The third eigenvalue of the normal form of the fold ( $A_2$ ) singularity equals  $-1$  in the origin. The derivative of the eigenvalue field in the direction of the corresponding eigenvector field does not vanish in the origin. The normal form thus satisfies the caustic conditions of the fold singularity. The normal forms of the remaining singularities follow analogously.